Native H_2 exploration in the western Pyrenean foothills

Nicolas Lefeuvre[1,2,*], Laurent Truche[1], Frédéric-Victor Donzé[1], Maxime Ducoux[3], Guillaume Barré[2,4], Rose-Adeline Fakoury[2], Sylvain Calassou[2], Eric C Gaucher[2]

[1] Université Grenoble Alpes, CNRS, ISTerre, F-38058 Grenoble Cedex 9, France

[2] Total SA, CSTJF, F-64018 Pau Cedex – France

[3] M&U SAS, 38120 Saint-Egrève - France

[4] Université de Pau et Pays de l'Adour, E2S UPPA, CNRS, Total, LFCR, 64000, PAU, France

[*]Corresponding author: Nicolas Lefeuvre (nicolas.lefeuvre@univ-grenoble-alpes.fr)

Key Points:

- Soil gas mapping for H_2 targeting
- Fertile area for H_2 production, migration
- Multiple gas analysis

Abstract:

Native hydrogen (H_2) may represent a new carbon free energy resource, but to date there is no specific exploration guide to target H_2-fertile geological settings. Here, we present the first soil gas survey specifically designed to explore H_2 migration in a region where no surface seepage has been documented so far. We choose the Pyrenean orogenic belt and its northern foreland basin (Aquitaine, France) as a playground to test our strategy. The presence of a mantle body at shallow depth (<10 km) under the Mauléon Basin connected to the surface by major faults is considered as a preliminary pathfinder for H_2 generation and drainage. On this basis, more than 1,100 in situ soil gas analysis (H_2, CO, CO_2, CH_4, H_2S, and ^{222}Rn) were performed at ~1 m depth at the regional scale along a 10 × 10 km grid spanning over 7,500 km^2. The analysis campaign reveals several hot spots to the north of the Mauléon Basin where H_2, CO_2 and ^{222}Rn concentrations exceed 1000 ppmv, 10 vol% and 50 kBq m^{-3}, respectively. Most of these hot spots are located along the North Pyrenean Frontal Thrust and other related faults rooted in the mantle body. These results, together with evidence of fluid migration at depth, suggest that H_2 may be sourced from mantle rocks serpentinization and carried to the surface along major thrusting faults. Hydrogen traps remain unidentified up to now but the presence of salt-related structures (diapirs) near these hot spots could play this role.

Plain language Summary:

Native hydrogen (H2) is currently considered as a possible energy resource for the development of a carbon-free society. Throughout the world, and for over a century, numerous natural H2-bearing geological fluids have been discovered, but to date, there is neither exploration strategy nor any resource assessment, as practical guidelines for hydrogen targeting are still missing. Here, we propose a new integrated approach dedicated to native H2 exploration, using the Pyrenean orogenic belt and its northern foreland basins as a playground. On this basis, a soil gas (H2, CO2, CH4, radon) exploration campaign, encompassing the major tectonic structures identified in the region has been carried out. This survey reveals several hotspots where H2, CO2 and radon concentrations are by two orders of magnitude above the regional background. These hotspots are mainly located along major faults deeply rooted in the mantle body (~10 km depth) that is well imaged by geophysical data. Therefore, the combined presence of soil gases significantly enriched in H2, CO2, and radon, a dense mantle body below the foreland basin potentially subject to active hydrothermal alteration, and deep faults, represents a favorable geological setting for H2 generation and drainage.

1 Introduction

Several water-rock interaction processes producing molecular hydrogen (hereafter "hydrogen" or "H_2") in the Earth are now well identified (Klein et al., 2020). Among these processes, serpentinization of ultramafic rocks (Malvoisin et al., 2011; Marcaillou et al., 2011; Mayhew et al., 2013; McCollom et al., 2016) and water radiolysis (Lin et al. 2005a; Truche et al., 2018) have drawn most of the scientific attention so far because they may fuel deep microbial subsurface ecosystems and trigger the abiotic synthesis of organic molecules (Etiope et al., 2015; Fiebig et al., 2007; Johnson et al., 2015; Lin et al., 2005b; McCollom, 2013; Sauvage et al., 2021; Schrenk et al., 2013; Sherwood Lollar et al., 2006; Sherwood Lollar et al., 2021; Truche et al., 2020; Vandenborre et al., 2021). Recently, the growing demand for carbon-free energy has sparked an unprecedented interest in naturally occurring H_2, as it could represent a potential alternative resource to fossil fuels (Donzé et al., 2020;

Gaucher, 2020; Murray et al., 2020; Prinzhofer et al., 2018; Truche and Bazarkina, 2019, Smith et al., 2005).

The discoveries of hundreds of natural H_2 seepages, generally connected with circulation of hydrothermal fluids through ultramafic rocks both through seafloors (Donval et al., 1997; Charlou et al., 2010) and on continents (Abrajano et al., 1988; Deville & Prinzhofer, 2016; Monnin et al., 2009; Neal & Stranger, 1983; Vacquand et al., 2018; Zgonnik et al., 2020), raise important questions regarding the energy potential of natural hydrogen. Current estimates of global H_2 flux, even if poorly constrained (reported value ranges from ~0.2 to 2.1 Tg yr^{-1}; Cannat et al., 2010, Charlou et al., 2010; Merdith et al., 2020; Sherwood Lollar et al., 2014; Truche et al., 2020; Worman et al., 2020) seems to be too low to support an industrial production (~70 Tg of H_2 are manufactured annually worldwide). However, the recent observations of intra-cratonic seepages with no obvious relationship with ultramafic formations (Donzé et al., 2020; Larin et al., 2014; Moretti et al., 2021; Prinzhofer et al., 2019; Zgonnik et al., 2015) have challenged our understanding of H_2 production and behavior in the crust. Despite these questionings, the recent discovery of a H_2-rich (>90 mol% H_2), over-pressurized gas field from the shallow Bougou-1 well, Taoudeni Basin, Mali (Prinzhofer et al., 2018) that is used for small-scale electricity generation, attests to the niche potential of commercial H_2 exploitation.

Currently, there is neither specific exploration guide to target H_2 fertile geological settings, nor robust resource assessment that can promote industrial interests. Identification of circular depressions in intra-cratonic basins, ultramafic bodies exhumed at the surface (e.g. ophiolites, greenstones belts) or buried under a sedimentary cover represents a promising starting point for exploration, but our knowledge of the hydrogen system is still insufficient to design on purpose drilling campaigns based solely on this information. A combination of geophysical, geochemical and geological data is definitively needed, but in the absence of clearly established exploration guidelines, the direct detection of H_2 seepages remains one of the most straightforward and effective pathfinders. Indeed, the existence of focused seepages at the surface testifies to the presence of active H_2 flux driven by conduits or faults connecting potential leaking reservoirs or draining diffuse sources at depth. This can be done visually by observing H_2-rich gas bubbles in rivers or streams (Chavagnac et al., 2013; Deville et al., 2011), or eternal flame burning H_2 like in Chimaera, Turkey (Etiope et al., 2011), but also by monitoring soil gas emissions. Such a technique has already proven to be useful for the detection of H_2 degassing in surface rounded depressions located in intra-cratonic basins (Donzé et al., 2020; Larin et al., 2014; McCarthy et al., 1986; Moretti et al., 2020; Prinzhofer et al., 2019; Zgonnik et al., 2015). Soil gas monitoring (e.g. ^{222}Rn, He, CH_4, CO_2, COS, CS_2, H_2S and light hydrocarbons) combined with geophysical methods enables large areas survey and has already been applied with great success for targeting mineral, geothermal, and hydrocarbons resources (Disnar & Gauthier, 1988; Gao et al., 2011; Hinkle, 1994; McCarthy and Reimer, 1986; Noble et al., 2018; Pereira et al., 2010; Polito et al., 2002). Furthermore, the geochemical characteristics and behavior of soil gases (^{222}Rn, Hg, He, H_2, H_2S and CO_2) in volcanic and seismically active areas have been investigated widely for correlating geochemical variations with faults and earthquake activities (Ciotoli et al., 1999, 2007; Du et al. 2008; Li et al., 2013; Lombardi & Voltattorni, 2010; Wiersberg & Erzinger, 2008; Woodruff et al., 2009; Xiang et al., 2020).

Here, we present the results of a soil gas regional monitoring campaign dedicated to H_2 exploration. Following synergies and results from the Convergence project, we use the Pyrenean orogenic belt and his northern foreland basins as a case study. This area gathers several promising characteristics that may define a H_2-fertile geological province such as the presence of mantle rock at shallow depth connected to the surface by several deeply rooted faults. The objective of this study is to identify the presence of a H_2 fertile zone through the

direct observation of H_2 and associated gas (CH_4, CO_2, ^{222}Rn) emissions, and the comparison of soil gas maps with georeferenced structural and geophysical data.

2 Targeting H_2 emissions in the NW Pyrenees foothills

The Pyrenees is an E-W-trending orogenic belt (Fig. 1) resulting from the inversion of a series of rift basins that formed along the Iberia-Europe divergent boundary during the late Jurassic to Early Cretaceous time (e.g., Clerc et al., 2012, 2013; Ducoux et al., 2019; Jammes et al., 2009, 2010a; Lagabrielle and Bodinier, 2008; Lagabrielle et al., 2010; Lagabrielle et al., 2016; Lescoutre and Manatschal, 2020; Masini et al., 2014; Mouthereau et al., 2014; Teixell et al., 2018; Tugend et al., 2014, 2015b).

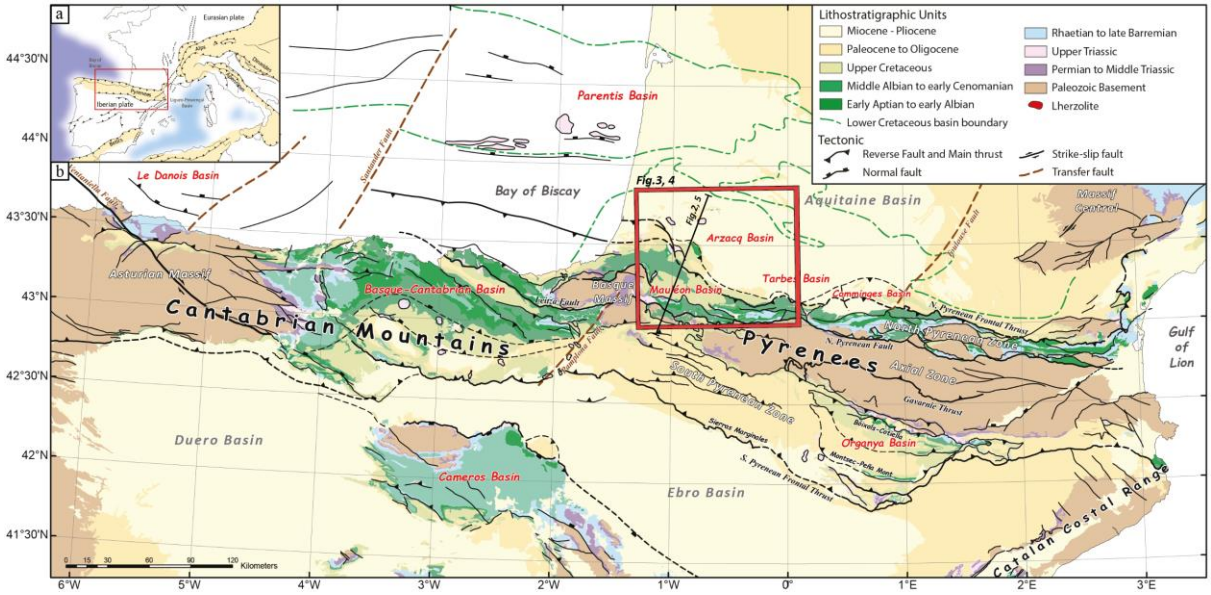

Figure 1. Tectonic setting of the Pyrenean-Cantabrian belt (modified from Pedrera et al., 2017 and Ducoux et al., 2019). (a) insert show the Iberian Peninsula and the Pyrenean belt in-between France and Spain. (b) Geological map of the Cantabrian Mountains and the Pyrenees, with location of the studied area (red rectangle) displayed on Figures 3 and 4. The black line corresponds to the trace of the cross section displayed on Figure 2 and 5.

After the Variscan orogeny, this area records several extensional phases, but the main phase of divergence between the Iberian and European plates occurs during early Aptian to early Cenomanian time. This main phase of divergence leads to hyperextension and mantle exhumation as suggested by remnants of rift basins and several pieces of mantle exposures now exposed in the North Pyrenean Zone (NPZ) of the Pyrenees (e.g. Jammes et al., 2009; Clerc et al., 2012, 2013; Fabries et al., 1991, 1998; Lagabrielle and Bodinier, 2008; Lagabrielle et al., 2016; Masini et al., 2014; Tugend et al., 2014; 2015b). Hyperextension and mantle exhumation related to a major lithospheric thinning were evidenced by a high temperature and low pressure metamorphism (Azambre and Rossy, 1976; Bernus-Maury, 1984; Clerc and Lagabrielle, 2014; Clerc et al., 2015; Dauteuil and Ricou, 1989; Ducoux et al., 2019; Golberg and Leyreloup, 1990; Lescoutre et al., 2019; Ravier, 1959) as well as emplacements of alkaline magma along the rift axis (Azambre and Rossy, 1976; Azambre et al., 1992; Le fur-Ballouet, 1985; Rossy et al., 1992). The end of rifting was rapidly followed by the onset of contractional deformation during the late Santonian with the deposition of the early-orogenic sequence related to the inversion of the hyperextended rift system (García-Senz 2002; Garrido-Megias & Rios 1972; Gómez-Romeu et al., 2019; McClay et al., 2004; Mouthereau et al., 2014; Muñoz, 1992; Teixell, 1998; Vergés et al., 1995; Vergés & García-Senz, 2001). The main convergence phase (i.e. collision) occurred in Eocene-Oligocene times

(Mouthereau et al., 2014; Muñoz 1992, 2002; Vergès et al. 2002) and ended during the Chattian (Ortiz et al., 2020). The present-day structure of the Pyrenean belt (Fig. 2) shows an asymmetric double-verging tectonic wedge composed of Paleozoic rocks above the northward underthrusting Iberian continental lithosphere inherited from the Cretaceous hyperextended Pyrenean rift system (e.g., Chevrot et al., 2018; Choukroune and ECORS Team, 1989; Mouthereau et al., 2014; Muñoz, 1992; Roure et al., 1989; Teixell, 1998; Teixell et al., 2016; Vergés et al., 1995; Wang et al., 2016; Fig. 2)..

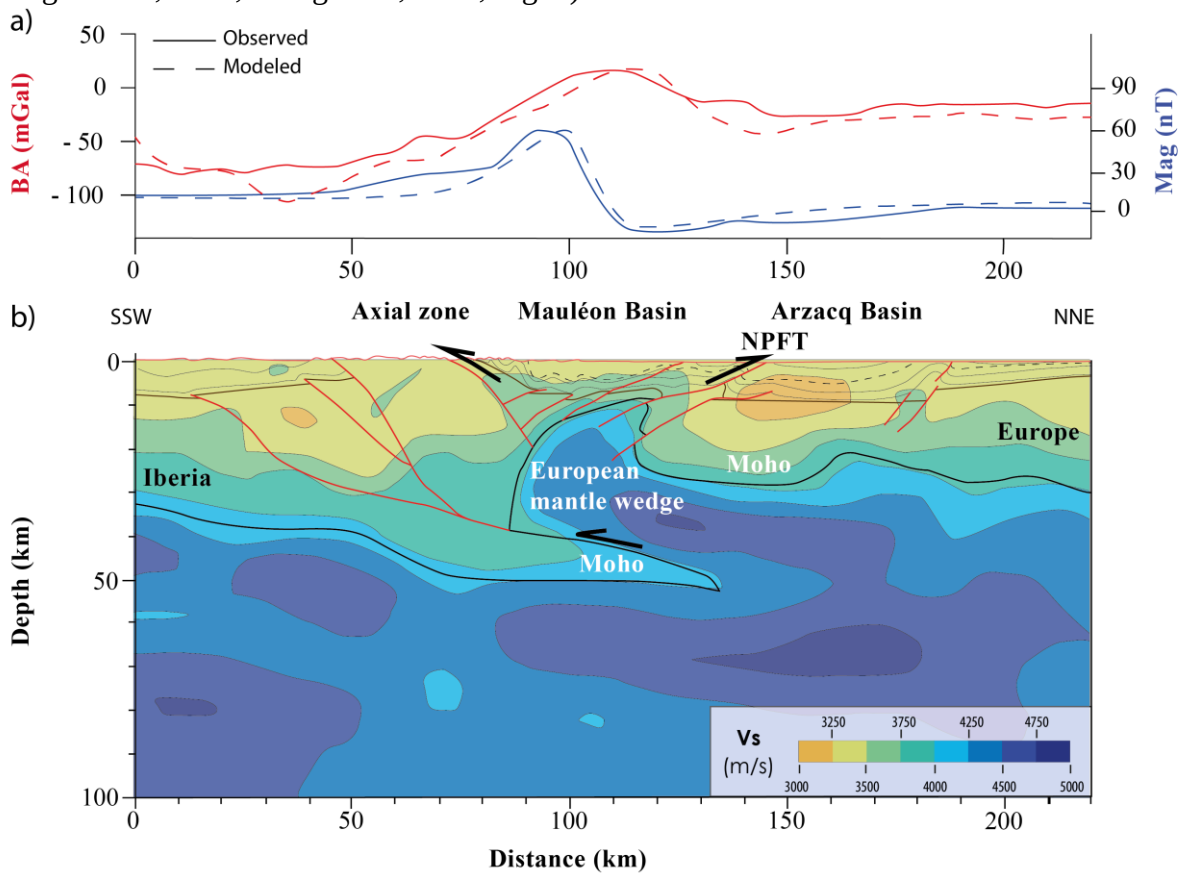

Figure 2. (a) Bouguer (Ayala et al., 2016) and magnetic anomalies (García-Senz et al., 2019), and (b) Vs model obtained by full waveform inversion (modified from Wang et al., 2016) along the same transect shown in Figure 1. NPFT – North Pyrenean Frontal Thrust

In this study we focus on the Mauléon and Arzacq Basins, located in the western NPZ of the Pyrenees. During the rifting phase, these two rift basins bounded by detachment faults were separated by the Grand Rieu ridge made of Paleozoic basement (Jammes et al., 2009; Lecoutre et al., 2019; Masini et al., 2014; Saspiturry et al., 2020; Tugend et al., 2014). The Arzacq Basin sat on the hyperthinned continental crust whereas the Mauléon Basin lied directly on top of exhumed mantle. At present-day, the rift architecture of the Arzacq Basin is relatively well preserved, while the Mauléon Basin was highly deformed during subsequent orogenesis. This latter corresponds to a pop-up structure (e.g., Labaume and Teixell, 2020; Teixell et al., 2016;) that overthrusts the Arzacq Basin towards the north along the North Pyrenean Frontal Thrust (NPFT) and the Axial Zone towards the south along the North Pyrenean Fault (NPF) (Fig. 2b).

Several geophysical studies have also revealed interesting characteristics of the deepest structure of the western Pyrenees (i.e. beneath the Mauléon Basin) by processing gravimetric (Lacan, 2008), magnetic (Garcia-senz et al., 2019) and seismic data (Chevrot et al., 2015, 2018; Wang et al., 2016). First, a strong positive Bouguer gravity anomaly (> 20 mGal; Fig. 2) is observed below the Mauléon Basin. This anomaly is interpreted as the

presence of dense materials at relatively shallow depth such as lower crust or mantle pieces (Grandjean, 1994; Pedreira et al., 2007, Pedrera et al., 2017; Vacher & Souriau, 2001). Second, a significant positive magnetic anomaly (> 60 nT; Fig. 2) is located right below the Mauléon Basin (Garcia-Senz et al., 2019). This magnetic anomaly, which is well correlated with the Bouguer anomaly previously mentioned, provides key information on the nature of mantle rocks because the magnetic susceptibility might be correlated to the serpentinization degree (Oufi et al., 2002; Toft et al., 1990). Indeed, the ultra-mafic rocks such as lithospheric mantle acquire their para-magnetism during the serpentinization reaction, and the associated formation of magnetite. Third, high seismic velocities ($Vp \approx 7.3$ km s^{-1}, $Vs \approx 4.2$ km s^{-1}) were calculated by full waveform inversion under the western part of Mauléon Basin and are attributed to an exhumed serpentinized mantle body located at 8 to 10 km depth (Christensen, 2004, Wang et al., 2016).

All together, these geophysical data support the presence of a dense mantle body at ~8 km depth below the Mauléon Basin inherited from the Cretaceous pre-collision hyperextended rift system. This dense mantle body was further incorporated into the accreting wedge during the orogenesis of the Pyrenean belt (e.g. Casas et al., 1997; Jammes et al., 2010a; Wang et al., 2016; Lescoutre and Manatschal, 2020; Saspiturry et al., 2020). Therefore, the combination of all these data indicating both the presence of a potential source of H_2 through mantle rocks serpentinization and the existence of preferential conduits for fluid migration makes the north Pyrenean foothills a promising geological setting for H_2 exploration.

3. Materials and Methods

3.1 Soil gas analysis

The investigated area for soil gas analysis is located in the southwest of France (Aquitaine region) along the Pyrenean belt and corresponds to approximately 7500 km² (Fig. 1). It encompasses the NPZ, the Mauléon Basin, the Arzacq Basin and the Grand Rieu ridge. A total of 1106 soil gas in-situ measurements have been performed over 131 different locations (Table A2). The sampling mesh was defined along a ~10 × 10 km grid (Fig. 3a). The concentration and nature of gases measured in soils may vary according to meteorological (e.g. temperature, hygrometry) and pedological factors (e.g. soil composition, vegetation, microbiology). The present regional soil gas survey is not intended to document the effect of such parameters on soil gas composition. However, all the measurements have been done during spring and summer seasons (April to August 2018, 2019 and 2020) in order to limit the amplitude of hygrometry and temperature variation. Soils affected by anthropogenic activities, such as ploughed soils, gardens or industrial areas have not been sampled. Most of the sampling sites located to the western part of the NPZ have altitudes between 50 to 400 meters above sea level and are mainly composed of grasslands and forest soils. The sampling sites located in the Axial Zone have altitudes ranging from 400 to 1500 meters and are mostly composed of forests and meadows.

At each sampling site, 7 small boreholes were drilled in the soil over an area of 100 m^2 - 5 of them were devoted to H_2, CO, CO_2, CH_4, H_2S, and O_2 measurement using a GA-5000 (GeoTech®) multi-gas analyzer and the remaining 2 were dedicated to radon (^{222}Rn) measurement using an AlphaGuard DF2000 radon analyzer (Bertin instrument®). Additional series of measurements have been carried out over time (2018, 2019 and 2020) on hot spots where H_2 concentration was > 200 ppmv. Each borehole has a depth of ~1 m and a diameter of 1 cm. A portable drill (DH36DBL, Hitachi®) operating in percussion mode only (no rotation of the drill bit) was used for this purpose. Numerous tests were conducted using various drilling procedures on different lithologies and soils to determine the optimal drill

configuration. Thus, a specific drilling procedure was selected to minimize and even prevent any production of H_2 through drill bit metamorphism and "mechano–radical" processes. Indeed, the increase in temperature of the drill bit may induce the cracking of the organic matter and trigger H_2 production (Lewan et al., 1997; Li et al., 2017; Lorant et al., 2002). The mechanical dissociation of the covalent Si-O bond in silicate minerals creates surface radicals which react with water to produce H_2. This process, referred to as "mechano–radical", has been experimentally demonstrated by friction experiments involving various silicate bearing rocks saturated with water (Hirose et al., 2011) and is supposed to be at the origin of high concentration of H_2 in soil gas associated with active tectonic faults (Kita et al., 1982; Sato et al., 1984). Drilling boreholes in soils without drill bit rotation clearly prevent artificial generation of H_2 as demonstrated by Halas et al. (2021), and by our plethora of measurements where H_2 concentrations in soil gas is lower than 5 ppmv (Table A1). Immediately after drilling, a stainless-steel sampling probe was tightly inserted inside the borehole and connected to one of the two gas analyzers either for ^{222}Rn or for H_2, CO_2, CH_4 and O_2 measurements. Each gas analyzer is equipped with a pump set to operate at the same flow rate of 550 mL min^{-1}.

The multi-gas detector GA-5000 is equipped with two different sensors: 1) an electrochemical cell for H_2, CO, H_2S, and O_2 concentration measurements, and 2) a dual wavelength infrared sensor for CO_2 and CH_4 concentration measurements. Uncertainties and interferences are documented in Table 1. Galvanometric measurement of a gas mixture of H_2, CO, and H_2S is subject to potential cross-interferences (Korotcenkov et al., 2009).

Gas	Range	Typical accuracy	
CH_4	0 - 100 vol%	0 - 70 ± 0.5 vol%	70 - 100 ± 1.5 vol%
CO_2	0 - 100 vol%	0 - 60 ± 0.5 vol%	60 - 100 ± 1.5 vol%
O_2	0 - 25 vol%	0 - 25 ± 1 vol%	
H_2	0 - 1000 ppmv	2 ppmv	

Table 1. Gas concentration range and measurement accuracy for CH_4, CO_2, O_2 and H_2 analysis by the GA-5000 instrument.

However, H_2 concentration measurement over the 0 – 1000 ppmv range is weekly impacted (< 10 ppmv) by the combined presence of CO and H_2S provided their concentrations remain < 300 ppmv and < 15 ppmv, respectively. Other species like HCN, NO_x or C_2H_4 may also interfere with the H_2 measurement, but their concentrations have never been detected in the prospected soils. For all measurements done in the field, H_2S has never been detected in the soil gases during our exploration campaign, neither using the GA-5000 gas analyzer nor by gas chromatography (see below), nor olfactorily for H_2S (human can smell H_2S at few tens of ppb in the air). In addition, for every H_2 concentration recorded with the GA-5000 analyzer at a value above 500 ppmv, a separate soil gas sample was taken in a gas tight Swagelok® stainless steel gas cylinder (40 mL). The cylinder was put under vacuum first using a primary vacuum pump and then connected to the soil gas probe for sampling. The gas composition was further analyzed in the lab regarding H_2, CO_2, CO, CH_4 using a Perkin Elmer® CLARUS 500 Gas Chromatograph (GC) equipped with a thermal conductivity detector (TCD) and a 2 m long column (RESTEK® Shin Carbon ST 80/100) with Ar as a carrier gas. The GC was calibrated using several Ar + H_2 + CH_4 + CO_2 + CO gas mixtures of different concentrations injected with a gas syringe of calibrated volume. The estimated analytical error is ± 5%.

The AlphaGuard DF2000 device is equipped with a pulsed ionization chamber (internal volume of 0.62 L) and a fiberglass selective filter. The radon (^{222}Rn) measurement

range is between 2 to 2 $\times 10^6$ Bq·m^{-3} with uncertainty variability of 5 cpm at 100 Bq·m^{-3}. The analysis is based on the decay of ^{222}Rn to ^{218}Po resulting in the emission of α-particles which can be measured by the instrument. Relative humidity, atmospheric pressure and temperature are simultaneously measured.

3.2 Soil gas data processing

The statistics of the soil gas concentration sampled during the survey are reported in Table 2. The averaged concentrations of H_2, CO_2 and ^{222}Rn were then interpolated and mapped using ArcGIS Pro (ESRI®) geographical information software (GIS). The natural neighbor interpolation method was used to define lines of equiconcentration of H_2, CO_2 and Radon. This method is based on the Voronoï tessellation of our discrete set of spatial gas concentration measurements (Sibson, 1981).

Gas	N	Mean	Standard deviation	Min	Max
H_2 (ppmv)	1106	33	104	0	> 1000
CO_2 (vol%)	1106	0.85	1.2	0	10.5
^{222}Rn (Bq m^{-3})	893	1002	9343	0	57316

Table 2. Main statistics of soil gas data acquired during this study.

4 Results

4.1 Soil gas mapping

The localization of each sampling site is shown in Figure 3a (red cross). These 131 locations constitute a sampling grid where a total of 1106 soil gas analyses have been carried out over 3 years (Table A1). This sampling grid is superimposed to the geological map of the targeted area (Fig. 3a) and the associated H_2, CO_2, and ^{222}Rn gas concentration contour maps are also plotted (Fig. 3b, c and d, respectively). When looking at these 3 latter maps (Fig. 3b, c and d), one can observe that most of the highest H_2, CO_2, and ^{222}Rn concentrations are located along the NPFT or to the south of this major fault. In addition, these high gas concentration data define 12 hot spots, with some of them being superimposed.

4.2 Hydrogen

Regarding H_2 concentrations, their values range from 0 to > 1000 ppmv. Among the 1106 concentration values reported in Table A1, 958 data (87 %) are < 50 ppmv, 146 data (6 %) are ≥ 50 ppmv, with 73 data (7 %) being > 100 ppmv and 5 data being above the sensor saturation (1000 ppmv) of the GA-5000 instrument. The high H_2 concentration values can be grouped into three main hot spots (Fig. 3b). The most significant hot spot is located between a triangle defined by Orthez to the north east, Peyrehorade to the east and Sauveterre-de-Béarn to the south. In this zone (133 km^2), 10 neighboring sampling sites display mean H_2 concentration values above 50 ppmv. In more details, among 298 measurements carried out over 3 years in this area, 89 (30 %) display H_2 concentration above 50 ppmv. Four sampling sites exhibit high H_2 concentrations: Le Bourguet (up to 547 ppmv), north and east Baigts-de-Béarn (up to 734 and 481 ppmv, respectively), Sauveterre-de-Béarn (up to 632 ppmv) and Laborde (above the quantification limit of 1000 ppmv). At Sauveterre-de-Béarn, H_2 concentration was independently measured by GC and was found to be as high as 822 ppmv. The second hot spot is located to the south west of Asasp Arros. It corresponds to a single location where 5 independents gas measurements were > 50 ppmv. The third hot spot, located to the south of Pau, corresponds to two neighboring locations close to the NPFT. There, 6

independent measurements were > 50 ppmv of H_2 with a maximum value of 129 ppmv. In addition to these 3 H_2 hotspots, it was found that the soils surrounding two outcropping bodies of lherzolite at Urdach and Turon de La Técouère (red squares on Fig. 3b) also display high H_2 concentrations, but with high heterogeneities among the values. At Urdach, over the 9 measurements carried out, 2 were > 1000 ppmv. At Turon de la Técouère, 2 measurements were > 1000 ppmv, 18 measurements were in-between 100 and 800, and the other 11 were < 100 ppmv. These two locations are both very singular and very specific because of their geological context. Thus, they are not included into the interpolation in order to avoid bias in the interpretation of the map.

4.3 Carbon dioxide

Regarding the CO_2 concentrations, their values range from 0 to 10.3 vol% with the following distribution: 815 values (74 %) are ≤ 1 vol%, 233 values (21 %) are in the range 1 to 3 vol% range, and 58 values (5 %) are > 3 vol% with a maximum at 10.3 vol% (Table A1). The spatial distribution of CO_2 concentration is less contrasted than for H_2, but the high concentrations zones lie mostly to the south of the NPFT (Fig. 3b). Among the five detected hotspots where CO_2 concentration exceed 3 vol%, one display some overlaps with the previously described H_2 hot spot located on the NPFT: i.e. close to Peyrehorade with a maximum of 3.05 vol%. Another was located near Sauveterre-de-Béarn with a maximum of 10.3 vol%. Two others hot spots were located along faults, to the east of Asasp-Arros, and to the south-east of Lourdes. Their maximum CO_2 concentrations are 2.9 and 3.8 vol%, respectively. The last hot spot is located in the Arzacq Basin to the east of Orthez. It exhibits a maximum CO_2 concentration of 2.5 vol%.

4.4 Methane, carbon monoxide and hydrogen sulfide

Methane (CH_4) was also measured with the GA-5000 instrument, but its concentration was always below the quantification limits (0.5 vol%) and was not detected by GC analysis at Sauveterre-de-Béarn. Hydrogen sulfide (H_2S) was never detected, and carbon monoxide (CO) was rarely detected (38 values ≥ 10 ppmv, maximum 79 ppmv), with a random spatial distribution. The oxygen (O_2) concentration was very close to 20 vol% (except when CO_2 concentration was > 5 vol%) indicating that all our samples were dominated by air.

4.5 Radon

Finally, the radon soil gas map (Fig. 3d) can be nicely superimposed to the H_2 and CO_2 zones (Fig. 3b, and d, respectively). Among the 893 ^{222}Rn concentration values (Table A1), 177 (20 %) are ≥ 1 kBq m^{-3}, with a very high value of 57.3 kBq m^{-3} recorded at Sauveterre-de-Béarn. Most of the highest ^{222}Rn concentrations are located along the NPFT and to the south of this major fault. Seven hot spots exceeding ^{222}Rn concentration of 5 kBq m^{-3} can be easily identified: 1) Peyrehorade with a maximum at 28.6 kBq m^{-3}, 2) to the north of Sauveterre-de-Béarn with a maximum at 57.3 kBq m^{-3}, 3) to the north of Estérençuby with a maximum at 13.4 kBq·m^{-3}, 4) to the west of Asasp-Arros with a maximum of 33.2 kBq m^{-3}, 5) to the south of Asasp-Arros with a maximum at 20 kBq m^{-3}, 6) to the west of Lourdes with a maximum at 14.4 kBq m^{-3}, and 7) to the north-east and south-east of Maubourguet with maximums of 12 and 8.2 kBq m^{-3}, respectively. Interestingly, the large H_2 and CO_2 hotspot previously identified in between Orthez, Peyrehorade and Sauveterre-de-Béarn, also corresponds to an area of high ^{222}Rn concentration.

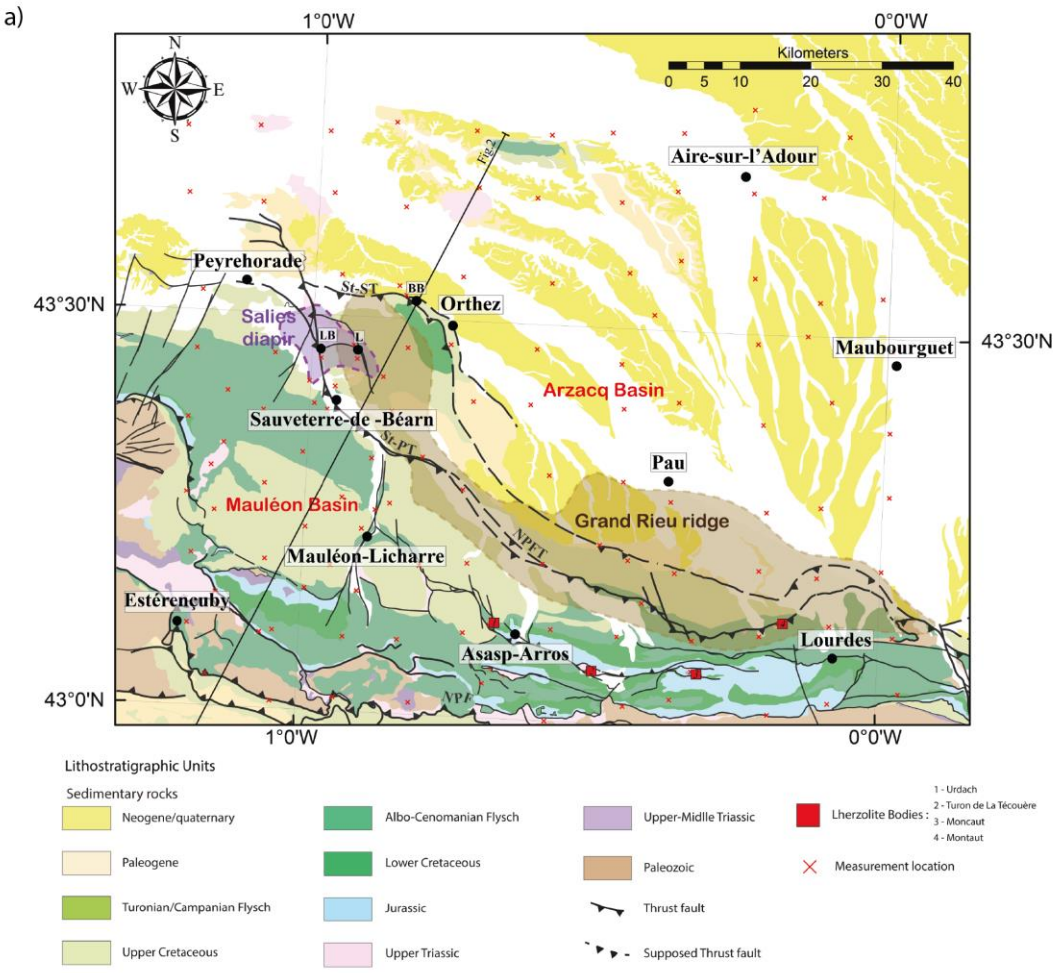
a)
1°0'W
0°0'W
43°30'N
43°0'N
N
S
W
E
Kilometers
0 5 10 20 30 40
Fig.2
Aire-sur-l'Adour
Peyrehorade
St-ST
BB
Orthez
Salies diapir
LB
L
Maubourguet
Arzacq Basin
Sauveterre-de -Béarn
St-PT
Pau
Mauléon Basin
Grand Rieu ridge
NPFT
Mauléon-Licharre
Estérençuby
Asasp-Arros
Lourdes
NPF
Lithostratigraphic Units
Sedimentary rocks
Neogene/quaternary
Paleogene
Turonian/Campanian Flysch
Upper Cretaceous
Albo-Cenomanian Flysch
Lower Cretaceous
Jurassic
Upper Triassic
Upper-Midlle Triassic
Paleozoic
Thrust fault
Supposed Thrust fault
Lherzolite Bodies :
1 - Urdach
2 - Turon de La Técouère
3 - Moncaut
4 - Montaut
Measurement location

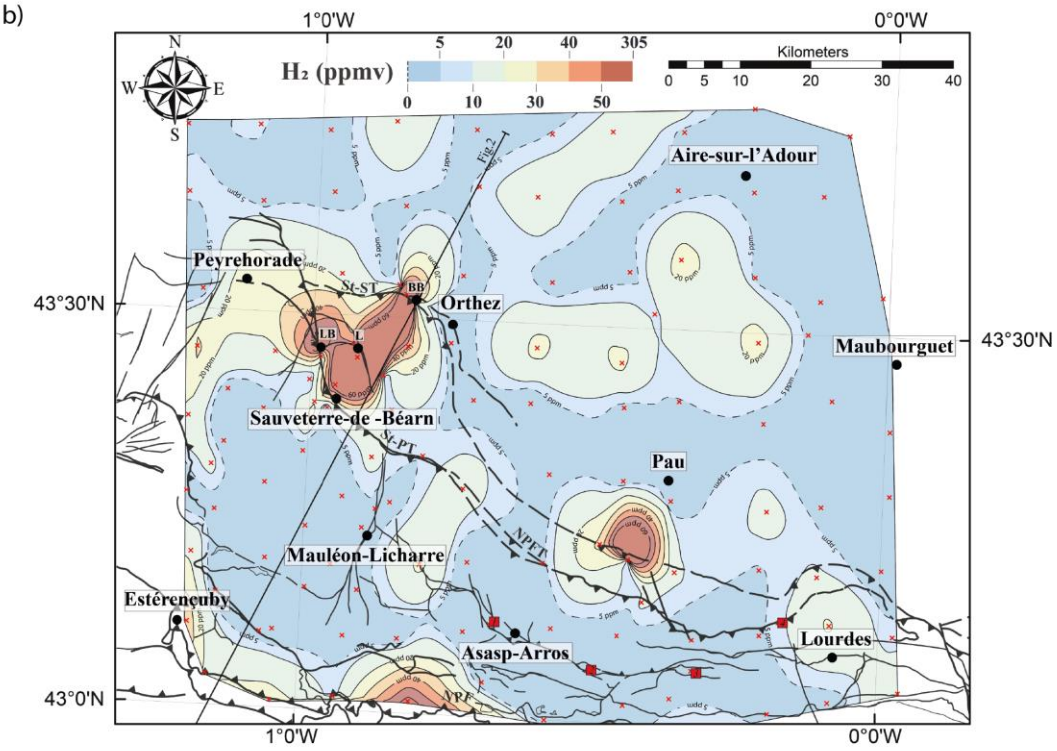
b)
1°0'W
0°0'W
43°30'N
43°0'N
N
S
W
E
H₂ (ppmv)
5 20 40 305
0 10 30 50
Kilometers
0 5 10 20 30 40
Fig.2
Aire-sur-l'Adour
Peyrehorade
St-ST
BB
Orthez
LB
L
Maubourguet
Sauveterre-de -Béarn
St-PT
Pau
NPFT
Mauléon-Licharre
Estérençuby
Asasp-Arros
Lourdes
NPF

c)

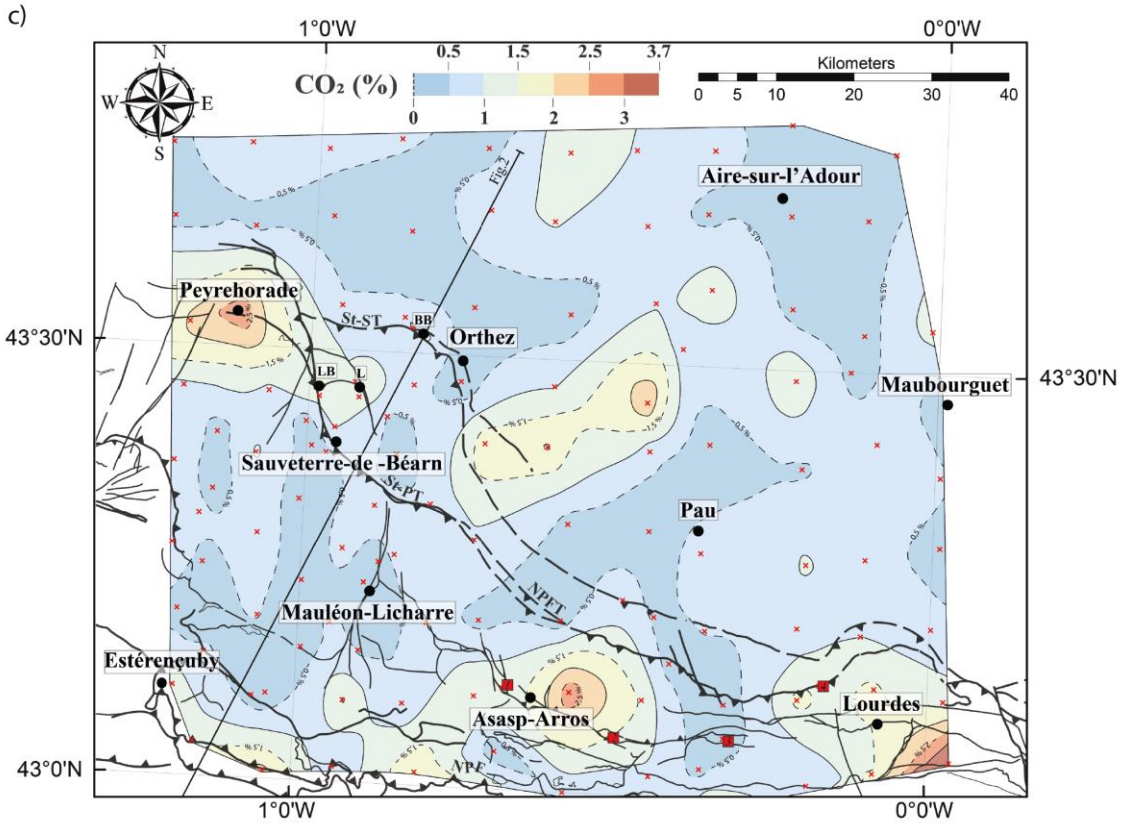
1°0'W
0°0'W
43°30'N
43°0'N
N
S
W
E
CO₂ (%)
0.5
1.5
2.5
3.7
0
1
2
3
Kilometers
0
5
10
20
30
40
Fig.2
Aire-sur-l'Adour
Peyrehorade
St-ST
BB
Orthez
LB
L
Maubourguet
Sauveterre-de -Béarn
St-PT
Pau
NPFT
Mauléon-Licharre
Estérençuby
Asasp-Arros
Lourdes
VPF

d)

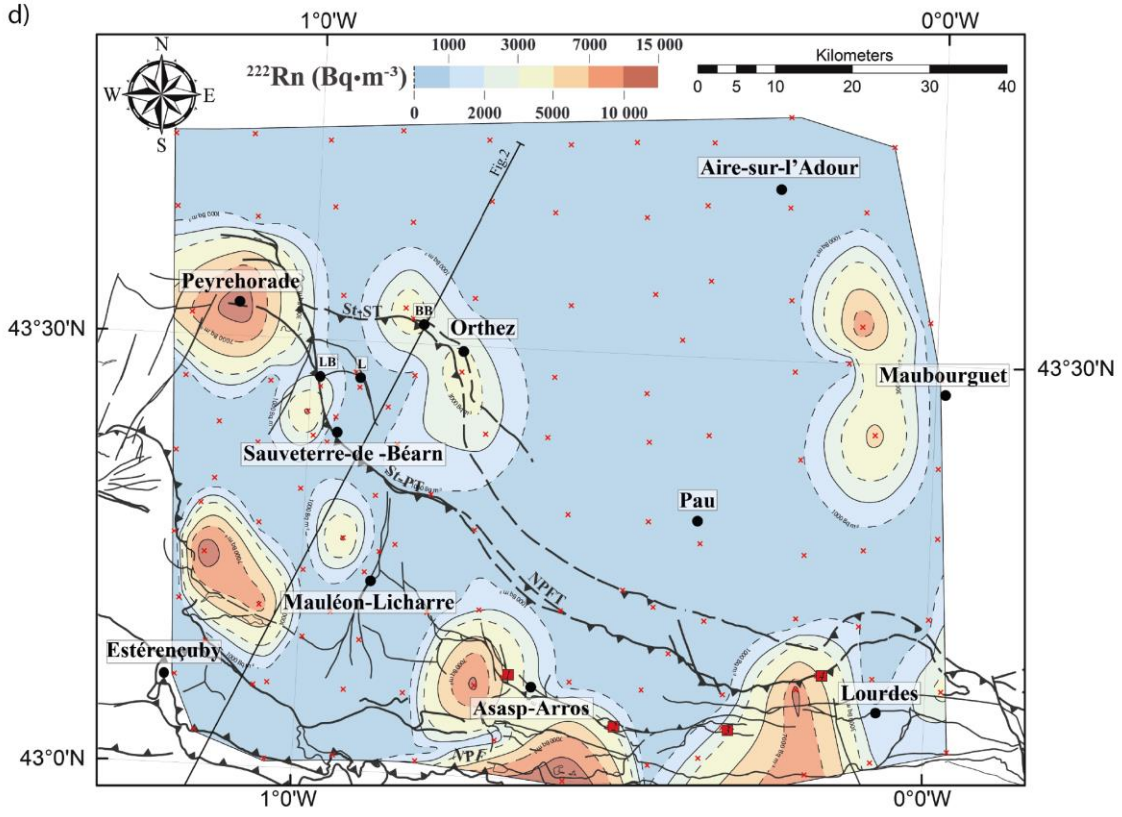
1°0'W
0°0'W
43°30'N
43°0'N
N
S
W
E
222Rn (Bq•m-3)
1000
3000
7000
15 000
0
2000
5000
10 000
Kilometers
0
5
10
20
30
40
Fig.2
Aire-sur-l'Adour
Peyrehorade
St-ST
BB
Orthez
LB
L
Maubourguet
Sauveterre-de -Béarn
St-PT
Pau
NPFT
Mauléon-Licharre
Estérençuby
Asasp-Arros
Lourdes
VPF

Figure 3. (a) Geological map of the studied area with the localization of the Mauléon and Arzacq Basins split apart by the Grand Rieu ridge and the NPFT faults networks (St-ST - Saint-Suzanne Thrust; St-PT - Saint-Palais Thrust; Ducoux et al., 2021). Each red cross corresponds to a measurement site. (b, c, and d) Contour maps of the mean concentration of H_2, CO_2 and ^{222}Rn soil gas measured at each sampling site, respectively.

5 DISCUSSION

5.1 Soil gas background concentration and identification of gas anomaly thresholds

Statistical information about the soil gas survey is reported in Table 2 (min, max, median, standard deviation). All the measurements were acquired under similar meteorological conditions and can be compared to atmospheric gases concentrations of ^{222}Rn (0.01 kBq m^{-3}), H_2 (531 ppb), and CO_2 (0.039 vol%) (Baubron et al., 2002; Novelli et al., 1999).

Given the multiple potential sources of gases and the variability of their concentrations with respect to the atmosphere, the soil gas anomaly thresholds cannot be determined in an absolute way but a statistical approach can provide fruitful information (Ciotoli et al., 2016). Here, the background level of the soil gas was determined from the quantile-quantile plot (Q-Q plot) as described by Sinclair (1991). This procedure requires the identification of both quasi-linear segments on a probability curve and inflection points between the different linear trends (Lombardi et al., 2010; Reimann et al., 2005). The intersection between the different straight lines corresponds to threshold values. It is a graphical method used to identify different gas population above the background level which will be presented and used in the following sections (Fig. 4).

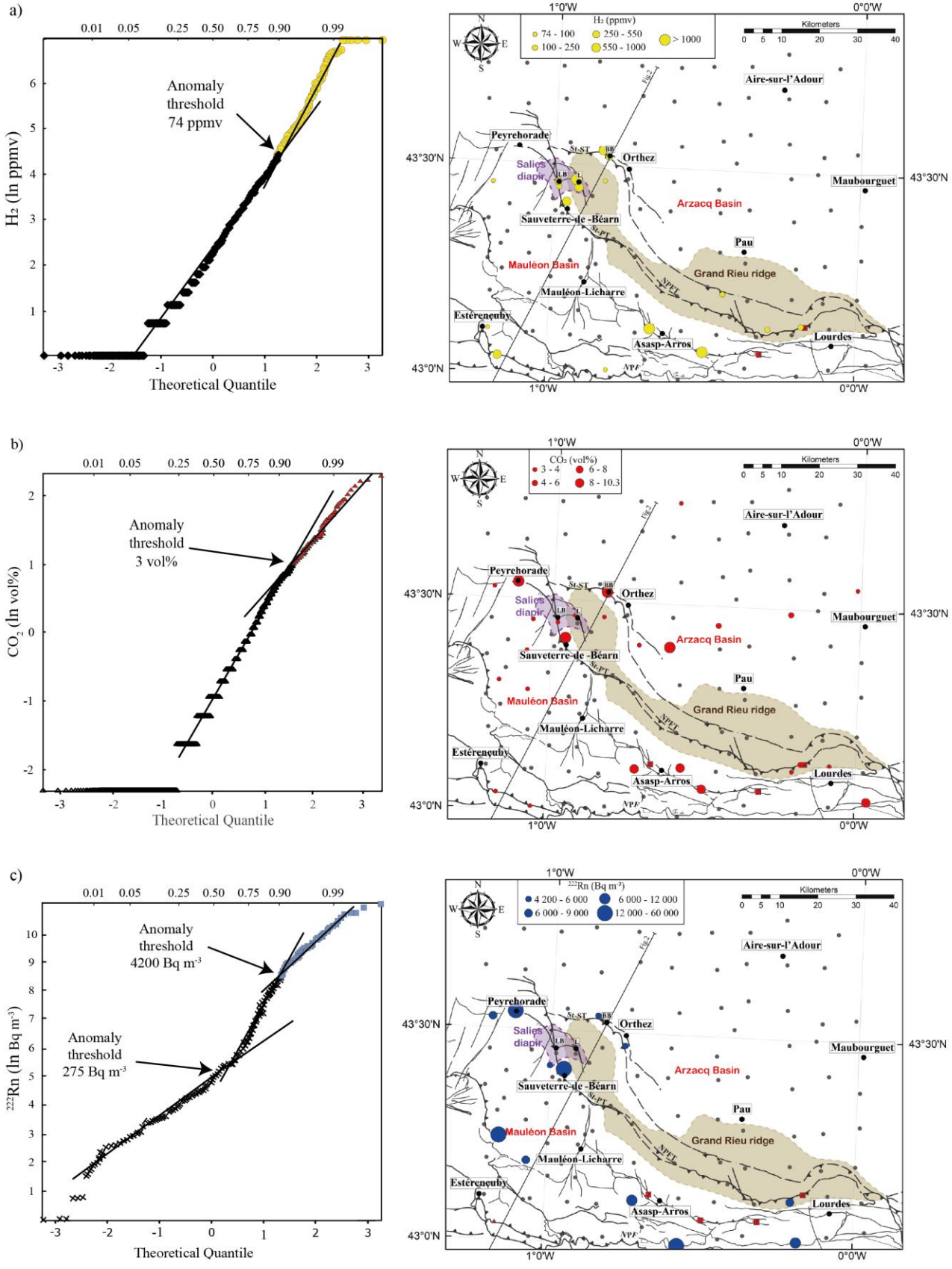
a)
0.01 0.05 0.25 0.50 0.75 0.90 0.99
Anomaly threshold 74 ppmv
H2 (ln ppmv)
Theoretical Quantile
H2 (ppmv)
74 - 100
100 - 250
250 - 550
550 - 1000
> 1000
Kilometers
Aire-sur-l'Adour
Peyrehorade
Orthez
Salies diapir
Maubourguet
Arzacq Basin
Sauveterre-de -Béarn
Pau
Mauléon Basin
Grand Rieu ridge
Mauléon-Licharre
Estérençuby
Asasp-Arros
Lourdes
1°0'W
0°0'W
43°30'N
43°0'N
b)
Anomaly threshold 3 vol%
CO2 (ln vol%)
CO2 (vol%)
3 - 4
4 - 6
6 - 8
8 - 10.3
c)
Anomaly threshold 4200 Bq m-3
Anomaly threshold 275 Bq m-3
222Rn (ln Bq m-3)
222Rn (Bq m-3)
4 200 - 6 000
6 000 - 9 000
6 000 - 12 000
12 000 - 60 000

Figure 4. On the left-hand side is shown the quantile-quantile plots (Q-Q plots) calculated for (a) H_2, (b) ^{222}Rn and (c) CO_2 soil gas measurements. The corresponding anomaly threshold values are 74 ppmv, 4,200 Bq m^{-3} and 3 vol%, respectively. The spatial distribution of these anomalies is displayed on the right-hand side of each Q-Q plots. NPFT – North Pyrenean Frontal Thrust; NPF – North Pyrenean Fault; St-ST - Saint-Suzanne Thrust; St-PT - Saint-Palais Thrust.

5.1.1 Hydrogen concentration anomalies

The Q-Q plot calculated for H_2 concentration highlights a non-linear evolution indicating the presence of at least two origins or sources for this gas (Fig. 4a). The inflection point between these linear trends indicates a soil gas concentration threshold anomaly at 74 ppmv.

The spatial distribution of H_2 concentrations is not random. Indeed, most of the measurements ranging from 1 to 74 ppmv (i.e. below the threshold) are located within the Arzacq and the Mauléon basins. The higher hydrogen concentrations (> 74 ppmv) are located near the main faults such as NPFT and NPF. The other anomalies, disconnected to these faults, are located close to the lherzolite bodies.

The hydrogen concentration below the threshold anomaly, i.e. the sharp change in concentration, could be linked to a microbial production. Microbial H_2 can be produced from different processes in soils such as fermentation, nitrogen fixation, anaerobic carbon monoxide oxidation or phosphite oxidation (Sipma et al., 2006; Schwartz et al., 2013). Hydrogen-producing microorganisms use metallo-enzymes such as [FeFe], [NiFe] and [Fe] hydrogenase in their metabolisms (Gregory et al., 2019). These enzymes can also be used in the reverse reaction for H_2 uptake and oxidation. These metallo-enzymes are present in anaerobic bacteria and eukaryotes (Peters et al., 2015). Fermentation is the most common process in nature to produce H_2 and may be important where organic matter is abundant. However, H_2 is usually maintained at low concentration in superficial environments because fermentative H_2 producer and respiratory H_2 consumers live in symbiosis or consortia in the microbial mats (Gregory et al., 2019, Kessler et al., 2019; Thauer et al., 1996). Thus, the net H_2 ecosystem flux is mainly controlled by soil uptake except during the leaf senescence in Autumn (Meredith et al., 2016). The optimum uptake temperature is approximately 30 °C (Ehhalt & Rohrer, 2011) and decreased with soil saturation, as water-filled pore spaces that prevent the gas diffusion (Conrad & Seiler, 1985; Popa et al., 2011). The type of soil is an important factor for both H_2 uptake and emission (Ehhalt & Rohrer, 2009). The uptake of H_2 is mainly related to the amount of hydrogenase in soil bacteria and to environmental conditions (Meredith et al., 2017). The rate of H_2 uptake is correlated to the abundance of H_2-oxidizing bacteria (Khdhiri et al., 2015). The highest uptake rates are recorded in forest soils while in grasslands the rates are lower (Chen et al 2015; Ehhalt & Rohrer, 2009; Khdhiri et al., 2015). Thus, the H_2 concentration in soils generally remains at low level, with lower values in forest soils than in grassland: 500 and 2500 ppb, respectively (Chen et al 2015). In this study, all H_2 concentration values below 10 ppmv can be the result of biological processes, while the high concentration values (> 74 ppm) reflect the contribution of other sources that may be deep-seated.

The hydrogen concentration ranging from 74 to > 1000 ppmv (i.e. above the threshold anomaly) seems to be clustered to the north west of Grand Rieu ridge and above the Salies salt diapir. These high H_2-concentrations may result from different sources than those below the threshold concentration value. They could be linked to mechano-radical reactions occurring along active faults or to a deeper production of H_2 through serpentinization, or water radiolysis. The rock crushing along fault plans results in the formation fresh surfaces that are extremely reactive. The reaction between these surfaces and water potentially

produces H_2 (Hirose et al., 2011; Kita et al., 1982). This mechanism is often invoked as the source of H_2 in active tectonic areas (Dogan et al., 2007). However, several studies have shown that the concentration of H_2 in the soil along active fault rarely exceed 100 ppm (Dogan et al., 2007; Li et al., 2013). Currently, the Pyrenean belt is in a post-orogenic situation, where earthquakes of low-magnitude occur currently. However, no earthquake with magnitude > 2.9 was recorded by the BCSF – RéNaSS seismic network near the surface along the NPFT during the sampling campaign. Thus, we can safely exclude rock comminution and mechano-radical process as major sources of H_2 in the targeted area. Therefore, others deep-seated origins for H_2, such as mantle rocks serpentinization or water radiolysis can be envisioned to explain the high H_2 concentration recorded near Sauveterre-de-Béarn. The role of deeply rooted faults in H_2 drainage is emphasized in the next section.

High concentration of H_2, i.e. > 1000 ppmv, are also recorded close to the two lherzolite bodies of Turon de la Técouère and Urdach (Table A1). The origin of these gas anomalies is probably not deep-sourced, but may correspond to low temperature serpentinization process, and to the release of gases entrapped in the rock as observed at a larger scale in numerous ophiolites worldwide (Etiope et al., 2011).

5.1.2 CO_2 concentration anomalies

The Q-Q plot calculated for CO_2 exhibits a non-linear evolution with an inflection point at 3 vol% that corresponds to a threshold anomaly (Fig. 4b). The CO_2 concentration below this value could be attributed to organic material oxidation, micro-organisms or plants respiration (Romanak et al., 2014; Sugisaki, 1983). The CO_2 concentrations above this threshold anomaly could result from a mixing of potential deep sources such as mantle degassing, carbonate metamorphism, or carbonate dissolution with other surface sources as describe above (Cooper et al., 1997).

The locations for CO_2 anomalies both in the basins and in fault zones are presented in Figure 4c. The anomalies observed in the basins are disconnected from the deep structure, which lead us to suppose that they are mainly the result of biological processes as detailed in the previous section. The others CO_2 anomalies are localized along faults (Fig. 4b) and are particularly clustered near the Salies diapir and to the north west of Grand Rieu ridge. These latter anomalies are also correlated with the H_2 and ^{222}Rn anomalies at this location. This clustering strengthens the scenario of an active gas-bearing fault zone where CO_2 acts as a carrier gas for other species (H_2 and ^{222}Rn) from deep-seated sources. Note that H_2 can also migrate independently from other gases because of the small size and high diffusivity of the molecule.

5.1.3 Radon concentration anomalies

The Q-Q plot calculated for ^{222}Rn also highlights a non-linear spatial evolution of its concentration with two inflection points indicating at least two possible threshold anomalies, the first at 275 Bq m^{-3} and the second at 4200 Bq m^{-3} (Fig. 4c). Radon concentrations below the first threshold anomaly at 275 Bq m^{-3} correspond to the background level in the area as described by the French Institute for Radioprotection and Nuclear Safety. Radon concentrations between 275 and 4200 Bq m^{-3} are randomly distributed above the sedimentary basins and generally located far from the faults. The radon concentrations above the second threshold anomalies (i.e. 4200 Bq m^{-3}) can be as high as 57 kBq m^{-3}. These high values are mainly localized along the faults (Fig. 4c) and more particularly to the north western part of Grand Rieu ridge, around the Salies salt diapir, where high H_2 concentrations are also recorded.Note that, The two anomalous values recorded within the core of the Mauléon Basin are the only exceptions to this distribution along faults of the high ^{222}Rn concentrations.

Because of its short half-life (3.82 days), ^{222}Rn must be carried rapidly upwards by ascending fluid to remain at high concentration when escaping into the atmosphere. Its presence at elevated concentration in soils indicates both active fluid circulation and subsurface lithologies enriched in ^{238}U, ^{232}Th and ^{40}K (Baubron et al., 2002). It has been already proven that ^{222}Rn is a useful pathfinder to map hydrothermal systems and active faults (Toutain & Baubron, 1999). Therefore, the high concentration of ^{222}Rn correlated with high H_2 and CO_2 concentrations near the Salies diapir, and along the NPFT near Sauveterre-de-Béarn, is a strong evidence for an active fluid circulation in deep-seated formations. Hydrogen may be at least partly sourced from water radiolysis, because these high ^{222}Rn concentrations testify for the presence of radioactive elements at depth.

5.2 Possible H_2 production system in the Pyrenean foothills

The western part of Pyrenean structure is characterized by a massive mantle body at shallow depth (< 10 km) as inferred from geophysical data (Chevrot et al., 2015, 2018; Garcia-Senz et al., 2019; Lacan, 2008; Wang et al., 2016). Another important observation is the occurrence of quasi-periodic seismic activity located to the south of the NPZ beneath the Mauléon Basin (Fig. 5). Numerous studies interpret these seismicity patterns as the result of stress triggered by fluid flows (Faulkner et al., 2010; Hainzl, 2004; Hardebeck, 2012; Rigo et al., 2008). Souriau et al. (2014) indicate that these earthquake clusters might be related to the convective circulation of fluids along the NPF (Fig. 5). Fluid circulation in deeply rooted faults is confirmed by helium and ^{222}Rn anomalies in soil gas (Baubron et al., 2002). Furthermore, the presence of fluid has been detected by low electrical resistivity at 13 to 15 km depths (Campanya et al., 2012). Such a depth also corresponds to the location of the seismic swarm identified by Souriau et al. (2014) (Fig. 5).

The regional geothermal gradient of 25.0 ± 2.7 °C km^{-1} (Bonté et al., 2010) is relatively modest, but the north western part of Mauléon Basin (Fig. 3a) displays anomalously high temperatures above 65 °C at 1000 to 2000 m depth. An indication of this thermal anomaly is the presence of numerous hydrothermal springs in the western part of Mauléon Basin; such as Combo-les-Bains, or Salies-de-Béarn. Hot fluid circulation may create a convection cell that drives heat upwards from deep thermal anomaly (Bonté et al., 2010). Given the regional geothermal gradient value, one may also expect temperatures at the top of the exhumated mantle at about 10 km depth to be around 250 °C (Saspiturry et al., 2020). Such a temperature is optimum for efficient serpentinization of the mantle rocks, magnetite formation, and H_2 generation (Malvoisin et al., 2011; Klein et al., 2020).

Therefore, the combined presence of both, a dense mantle body below the Mauléon Basin potentially subject to an active serpentinization, and deeply-rooted faults corresponding to the NPFT and the NPF zones (Fig. 2), represents a favorable geological setting for H_2 generation and drainage. Water radiolysis may also contribute to H_2 production, but to date we cannot discriminate this source from serpentinization. In the present case, we note however, that the importance of water radiolysis may be secondary compare to serpentinization in the global H_2 budget. Indeed, Warr et al. (2019) indicate that the contribution of water radiolysis on H_2 production is higher in felsic environments whereas its production by serpentinization comes mainly from mafic environments. Here, the presence of a large mantle body (i.e. ultra-mafic rocks) at shallow depth seems to provide the most fertile environment for H_2 generation. We therefore assume that H_2 is more likely generated by serpentinization than by radiolysis.

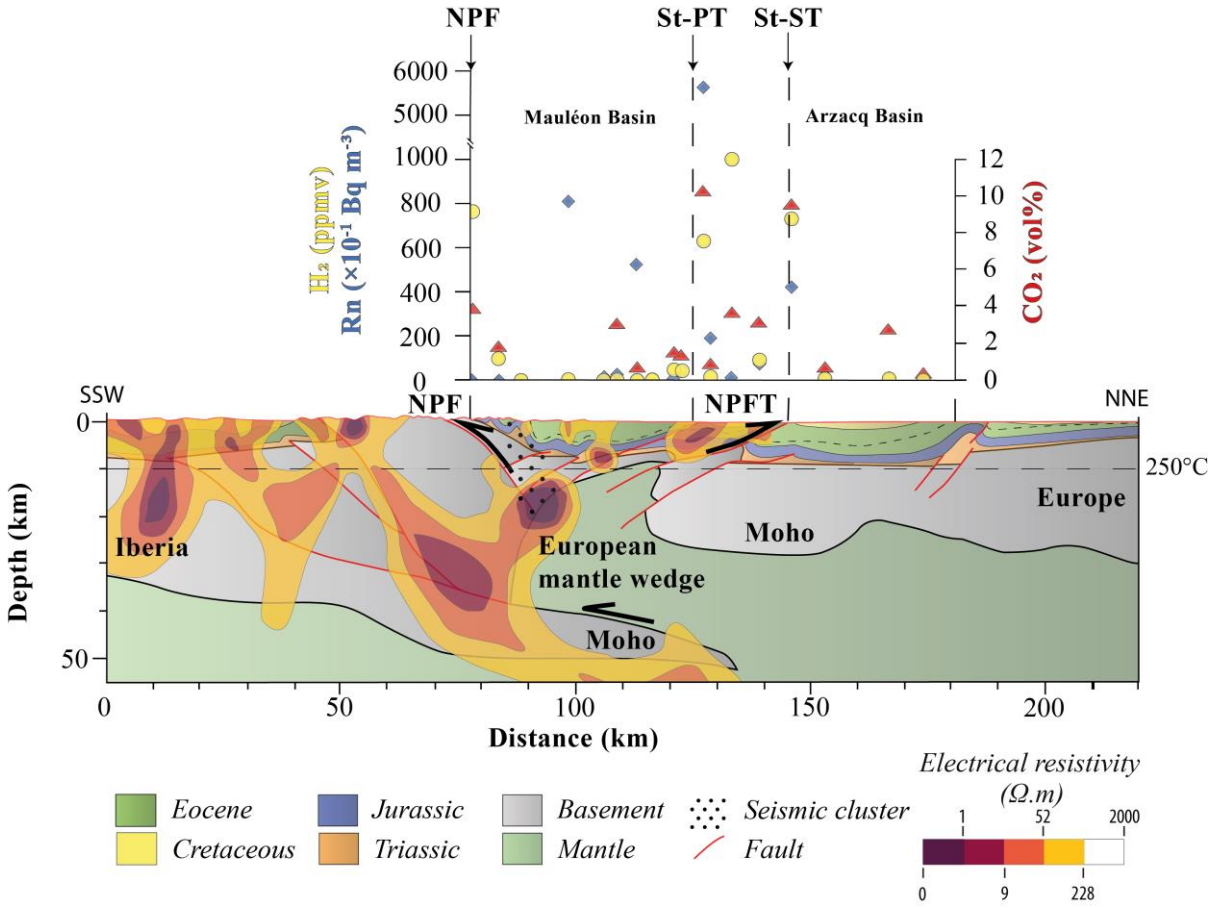

Figure 5. (bottom) Geological interpretation of the tomographic model (modified from Wang et al., 2016) superimposed to both a two-dimensional electrical resistivity model (after Campanyà et al., 2012) and the projection of a deep seismic cluster (after Souriau et al., 2014). The location of the section is shown on Figure 1. (top) H_2 (circle), ^{222}Rn (diamond) and CO_2 (triangles) max concentrations obtained along this section. NPFT – North Pyrenean Frontal Thrust; NPF – North Pyrenean Fault; St-ST - Saint-Suzanne Thrust; St-PT - Saint-Palais Thrust

In fact, the high H_2 emission spots obtained from the soil gas measurements carried out in the western Pyrenees agree well with the presence of this mantle body at shallow depth and the deep-rooted faults. The gas concentration along the western ECORS-Arzacq profile is displayed in Figure 5. The highest H_2, CO_2 and ^{222}Rn soil gas concentrations were recorded along the NPFT and the Grand Rieu ridge at >1000 ppmv, 10 vol%, and 57 kBq m^{-3}, respectively. Such deeply rooted faults, described as weakened zones partly composed of highly connected fracture networks, represent preferential pathways for fluid circulation carrying H_2 and other gases from deep sources to the surface (Baubron et al., 2002; Donzé et al., 2020; Gal & Gadalia, 2011). The gas concentration measurements carried out in the Mauléon and Arzacq Basins display lower values than within the Grand Rieu ridge (Fig 3a) and show a strong variability in concentration between H_2, CO_2 and ^{222}Rn. Hydrogen is nearly absent from these basins while the ^{222}Rn is only present in Mauléon Basin and CO_2 is present

in both basins. These basins were never connected during the Cretaceous rifting event, because they were separated separated by the Grand Rieu. The Arzacq Basin is therefore not connected to the mantle structure well identified below the Mauléon Basin (Masini et al., 2014; Lescoutre et al., 2019). Hence, these major structural features explain very well the contrasted in term of gas concentration patterns observed in-between these two basins.

In addition, the main hot spots located between Sauveterre-de-Béarn, Orthez and Peyrehorade are close to or just above the Salies salt diapir whose roof is only at less than 70 m below the surface (Berard & Mazurier, 2000). Such a structural configuration may also offer potential traps for deep-seated gases such as H_2. Indeed, salt formation is considered to offer the most promising option for large scale H_2 storage, because of their excellent sealing capacity and the relatively inert nature of salt with respect to H_2 (Sainz-Garcia et al., 2017; Tarkowski, 2019; Zivar et al., 2020). High H_2 concentrations (up to 30 vol%) have already been documented in evaporite formations and in particular in salt deposits (Warren, 2016). In salt formations, H_2 may have several origins like production during early biodegradation of organic matter, and water radiolysis due to elevated concentration of ^{40}K and ^{87}Rb, but the preponderant contribution of exogenic sources with subsequent migration into the evaporite trap is the most satisfying explanation.

6. Conclusions

Based on soil gas analysis and mapping we have discovered several hotspots of H_2, CO_2, ^{222}Rn where the concentration of these gases exceeds the regional background by two order of magnitude and more. The sampling sites of high H_2 concentration (> 1000 ppmv), together with CO_2 (up to 10 vol%), and ^{222}Rn (up to 60 kBq m^{-3}) are mostly located close to the North Pyrenean Frontal Thrust. The Crossing the information based on soil gas maps with different geophysical and geological datasets led us to identify a possible fertile environment for H_2 generation and drainage. First, outcrops of serpentinized peridotites in the NPZ are good indicator of the presence of exhumed mantle rocks at depth . Second, the geophysical observations reveal the presence of massive mantle body at shallow depth (< 10 km from tomographic, magnetic and gravimetric investigations) where active serpentinization may occur. Third, the H_2 and ^{222}Rn may be carried upward by CO_2 along major faults that connect the mantle body to the surface. The Salies salt diapir whose roof is only at less than 70 m below the surface represents an ideal gas trap for deep-seated gases such as H_2.

The discovery of these hotspots paves the way for detailed studies of noble gases and stable isotopes composition, but also for careful microbiological and pedological investigations to better constrain H_2 source(s) and migration path. The targeting approach deployed in our study may be applied elsewhere in the world and more particularly in orogenic belts presenting a geological configuration comparable to the western Pyrenean area. These orogenic areas, rich in ultramafic rocks, could be preferentially targeted for an industrial prospection of native H_2 resources.

Acknowledgments, Samples, and Data

This work was conducted in the framework of the Convergence project (https://convergent-margins.com/), funded by TOTAL S.E.. Magali Pujol, Dominique Duclerc and Isabelle Mitteau are warmly thanks for support during the field investigation and analytical measurements. Supplementary data reported in this study are given in supporting information and all soil gas data are stored in EarthChem repository at **pending (will be deposit after the review)**

Supplementary material

Table A1. All untreated soil gas data
Table A2. Average of soil gas data at each location

References

Abrajano, T. A., Sturchio, N. C., Bohlke, J. K., Lyon, G. L., Poreda, R. J., & Stevens, C. M. (1988). Methane-hydrogen gas seeps, Zambales Ophiolite, Philippines: Deep or shallow origin? *Chemical Geology*, *71*(1–3), 211–222. https://doi.org/10.1016/0009-2541(88)90116-7

Azambre, B., & Rossy, M., 1976, Le magmatisme alcalin d'age cretace, dans les Pyrenees occidentales et l'Arc basque; ses relations avec le metamorphisme et la tectonique. Bulletin de la Societe Geologique de France, S7–XVIII, 1725–1728. https://doi.org/10.2113/gssgfbull.S7-XVIII.6.1725

Azambre, B., Rossy, M., & Albarede, F., 1992, Petrology of the alkaline magmatism from the Cretaceous North-Pyrenean rift zone (France and Spain). European Journal of Mineralogy, 4, 813–834.

Baubron, J.-C., Rigo, A., & Toutain, J.-P. (1999). Soil gas profiles as a tool to characterise active tectonic areas: the Jaut Pass example (Pyrenees, France). *Earth and Planetary Science Letters*, 13. https://doi.org/10.1016/S0012-821X(01)00596-9

Berard, P., Mazurier, C. (2000) Ressources en eaux thermales et minérales des stations du département des Pyrénées-Atlantiques. Station thermale de Salies-de-Béarn. *Rapport BRGM/RP 50176-FR*

Bernus-Maury, C., 1984, Etude des paragenèses caractéristiques du métamorphisme mésozoïque dans la partie orientale des Pyrénées (French). Paris 6.

Bonté, D., Guillou-Frottier, L., Garibaldi, C., Bourgine, B., Lopez, S., Bouchot, V., & Lucazeau, F. (2010). Subsurface temperature maps in French sedimentary basins: new data compilation and interpolation. *Bulletin de La Société Géologique de France*, *181*(4), 377–390. https://doi.org/10.2113/gssgfbull.181.4.377

Cannat, M., Fontaine, F., & Escartín, J. (2010). Serpentinization and associated hydrogen and methane fluxes at slow spreading ridges. In P. A. Rona, C. W. Devey, J. Dyment, & B. J. Murton (Eds.), Geophysical Monograph Series (Vol. 188, pp. 241–264). Washington, D. C.: American Geophysical Union. https://doi.org/10.1029/2008GM000760

Casas, A., Kearey, P., Rivero, L., & Adam, C. R. (1997). Gravity anomaly map of the Pyrenean region and a comparison of the deep geological structure of the western and eastern Pyrenees. *Earth and Planetary Science Letters*, *150*(1–2), 65–78. https://doi.org/10.1016/S0012-821X(97)00087-3

Charlou, J. L., Donval, J. P., Konn, C., Ondréas, H., Fouquet, Y., Jean-Baptiste, P., & Fourré, E. (2010). High production and fluxes of H2 and CH4 and evidence of abiotic hydrocarbon synthesis by serpentinization in ultramafic-hosted hydrothermal systems on the Mid-Atlantic Ridge. In P. A. Rona, C. W. Devey, J. Dyment, & B. J. Murton (Eds.), *Geophysical Monograph Series* (Vol. 188, pp. 265–296). Washington, D. C.: American Geophysical Union. https://doi.org/10.1029/2008GM000752

Chavagnac, V., Monnin, C., Ceuleneer, G., Boulart, C., & Hoareau, G. (2013). Characterization of hyperalkaline fluids produced by low-temperature serpentinization of mantle peridotites in the Oman and Ligurian ophiolites: Hyperalkaline Waters in Oman and Liguria. *Geochemistry, Geophysics, Geosystems*, *14*(7), 2496–2522. https://doi.org/10.1002/ggge.20147

Chevrot, S., Sylvander, M., Diaz, J., Ruiz, M., Paul, A., & the PYROPE Working Group. (2015). The Pyrenean architecture as revealed by teleseismic P-to-S converted waves

recorded along two dense transects. *Geophysical Journal International*, *200*(2), 1094–1105. https://doi.org/10.1093/gji/ggu400

Chevrot, Sébastien, Sylvander, M., Diaz, J., Martin, R., Mouthereau, F., Manatschal, G., et al. (2018). The non-cylindrical crustal architecture of the Pyrenees. *Scientific Reports*, *8*(1), 9591. https://doi.org/10.1038/s41598-018-27889-x

Choukroune, P. (1989). The Ecors Pyrenean deep seismic profile reflection data and the overall structure of an orogenic belt. *Tectonics*, *8*(1), 23–39. https://doi.org/10.1029/TC008i001p00023

Christensen, N. I. (2004). Serpentinites, Peridotites, and Seismology. *International Geology Review*, *46*(9), 795–816. https://doi.org/10.2747/0020-6814.46.9.795

Ciotoli, G., Sciarra, A., Annunziatellis, A., & Bigi, S. (2016). Soil gas geochemical behaviour across buried and exposed faults dur- ing the 24 August 2016 central Italy earthquake. *ANNALS OF GEOPHYSICS*, 14. https://doi.org/10.4401/ag-7242

Clerc, C., Lagabrielle, Y., Neumaier, M., Reynaud, J. Y., & de Saint Blanquat, M., 2012, Exhumation of subcontinental mantle rocks: evidence from ultramafic-bearing clastic deposits nearby the Lherz peridotite body, French Pyrenees. Bulletin de la Société géologique de France, 183(5), 443-459.

Clerc, C., Boulvais, P., Lagabrielle, Y., & de Saint Blanquat, M., 2013, Ophicalcites from the northern Pyrenean belt: a field, petrographic and stable isotope study. International Journal of Earth Sciences, 103(1), 141-163.

Cooper, B. A., Raven, M. J., & Samuel, L. (1997). Origin and geological controls on subsurface CO2 distribution with examples from western Indonesia. *In Proceedings of the Petroleum Systems of SE Asia and Australasia Conference*, 877–92

Dauteuil, O., & Ricou, L. E., 1989, Une circulation de fluides de haute-temperature a l'origine du metamorphisme cretace nord-pyreneen. Circ. High-Temp. Fluids Orig. North Pyrenean Cretac. Metamorph. Geodinamica Acta, 3, 237–250.

Deville, E., & Prinzhofer, A. (2016). The origin of N2-H2-CH4-rich natural gas seepages in ophiolitic context: A major and noble gases study of fluid seepages in New Caledonia. Chemical Geology, 440, 139–147. https://doi.org/10.1016/j.chemgeo.2016.06.011

Disnar, J. R., & Gauthier, B. (1988). Exploration for concealed orebodies by the analysis of volatile organic compounds contained in surface rocks: Trèves Zn-Pb deposit (Gard, France), 18. https://doi.org/10.1016/0375-6742(88)90058-1

Dogan, T., Mori, T., Tsunomori, F., & Notsu, K. (2007). Soil H2 and CO2 Surveys at Several Active Faults in Japan. *Pure and Applied Geophysics*, *164*(12), 2449–2463. https://doi.org/10.1007/s00024-007-0277-5

Donzé, F.-V., Tsopela, A., Guglielmi, Y., Henry, P., & Gout, C. (2020). Fluid migration in faulted shale rocks: channeling below active faulting threshold. *European Journal of Environmental and Civil Engineering*, 1–15. https://doi.org/10.1080/19648189.2020.1765200

Donzé, F.-V., Truche, L., Shekari Namin, P., Lefeuvre, N., & Bazarkina, E. F. (2020). Migration of Natural Hydrogen from Deep-Seated Sources in the São Francisco Basin, Brazil. *Geosciences*, *10*(9), 346. https://doi.org/10.3390/geosciences10090346

Ducoux, M., Jolivet, L., Callot, J. P., Aubourg, C., Masini, E., Lahfid, A., ... & Baudin, T. (2019). The Nappe des Marbres unit of the Basque-Cantabrian Basin: the tectono-thermal evolution of a fossil hyperextended rift basin. Tectonics, 38(11), 3881-3915.

ECORS Team, Daignières, M., Séguret, M., & Specht, M. (1994). The Arzacq-Western Pyrenees ECORS Deep Seismic Profile. In A. Mascle (Ed.), *Hydrocarbon and Petroleum Geology of France* (pp. 199–208). Berlin, Heidelberg: Springer Berlin Heidelberg. https://doi.org/10.1007/978-3-642-78849-9_15

Ehhalt, D. H., & Rohrer, F. (2009). The tropospheric cycle of H2: a critical review. Tellus B: Chemical and Physical Meteorology, 61(3), 500-535.

Ehhalt, D. H., & Rohrer, F. (2011). The dependence of soil H2 uptake on temperature and moisture: a reanalysis of laboratory data. Tellus B: Chemical and Physical Meteorology, 63(5), 1040-1051.

Etiope, G., Judas, J., & Whiticar, M. J. (2015). Occurrence of abiotic methane in the eastern United Arab Emirates ophiolite aquifer. *Arabian Journal of Geosciences*, *8*(12), 11345–11348. https://doi.org/10.1007/s12517-015-1975-4

Etiope, Giuseppe, Schoell, M., & Hosgörmez, H. (2011a). Abiotic methane flux from the Chimaera seep and Tekirova ophiolites (Turkey): Understanding gas exhalation from low temperature serpentinization and implications for Mars. *Earth and Planetary Science Letters*, *310*(1–2), 96–104. https://doi.org/10.1016/j.epsl.2011.08.001

Etiope, Giuseppe, Schoell, M., & Hosgörmez, H. (2011b). Abiotic methane flux from the Chimaera seep and Tekirova ophiolites (Turkey): Understanding gas exhalation from low temperature serpentinization and implications for Mars. *Earth and Planetary Science Letters*, *310*(1–2), 96–104. https://doi.org/10.1016/j.epsl.2011.08.001

Fabriès, J., Lorand, J.-P., Bodinier, J.-L., & Dupuy, C., 1991, Evolution of the Upper Mantle beneath the Pyrenees: Evidence from Orogenic Spinel Lherzolite Massifs. Journal of Petrology, Special_Volume, 55–76. https://doi.org/10.1093/petrology/Special_Volume.2.55.

Fabriès, J., Lorand, J.-P., & Bodinier, J.-L. (1998). Petrogenetic evolution of orogenic lherzolite massifs in the central and western Pyrenees. *Tectonophysics*, *292*(1–2), 145–167. https://doi.org/10.1016/S0040-1951(98)00055-9

Faulkner, D. R., Jackson, C. A. L., Lunn, R. J., Schlische, R. W., Shipton, Z. K., Wibberley, C. A. J., & Withjack, M. O. (2010). A review of recent developments concerning the structure, mechanics and fluid flow properties of fault zones. *Journal of Structural Geology*, *32*(11), 1557–1575. https://doi.org/10.1016/j.jsg.2010.06.009

Fiebig, J., Woodland, A. B., Spangenberg, J., & Oschmann, W. (2007). Natural evidence for rapid abiogenic hydrothermal generation of CH4. *Geochimica et Cosmochimica Acta*, *71*(12), 3028–3039. https://doi.org/10.1016/j.gca.2007.04.010

Gal, F., & Gadalia, A. (2011). Soil gas measurements around the most recent volcanic system of metropolitan France (Lake Pavin, Massif Central). *Comptes Rendus Geoscience*, *343*(1), 43–54. https://doi.org/10.1016/j.crte.2010.11.008

Gao, Y., Wang, M., & Zhang, D. (2011). Application of 'metals-in-soil-gas' techniques to mineral exploration in exotic overburden. Geochemistry: Exploration, Environment, Analysis, 11(2), 63–70. https://doi.org/10.1144/1467-7873/09-IAGS-243

García-Senz, J., 2002, Cuencas extensivas del Cretacico Inferior en los Pireneos Centrales – formacion y subsecuente inversion. [PhD thesis]. University of Barcelona, Barcelona.

García-Senz, J., Pedrera, A., Ayala, C., Ruiz-Constán, A., Robador, A., & Rodríguez-Fernández, L. R. (2020). Inversion of the north Iberian hyperextended margin: the role of exhumed mantle indentation during continental collision. *Geological Society, London, Special Publications*, *490*(1), 177–198. https://doi.org/10.1144/SP490-2019-112

Garrido-Megias, A., & Rios Aragues, L. M., 1972, Sintesis geologica del Secundario y Terciario entre los rios Cinca y Segre (Pirineo Central de la vertiente sur pirenaica, provincias de Huesca y Lerida). Boletín Geológico y Minero, 83, 1–47.

Gaucher, E. C. (2020). New Perspectives in the Industrial Exploration for Native Hydrogen. *Elements*, *16*(1), 8–9. https://doi.org/10.2138/gselements.16.1.8

Golberg, J. M., & Leyreloup, A. F., 1990, High temperature-low pressure Cretaceous metamorphism related to crustal thinning (Eastern North Pyrenean Zone, France).

Contributions to Mineralogy and Petrology, 104, 194–207. https://doi.org/10.1007/BF00306443

Gomez-Romeu, J., Kusznir, N., Roberts, A., & Manatschal, G. (2020). Measurements of the extension required for crustal breakup on the magma-poor Iberia-Newfoundland conjugate margins. Marine and Petroleum Geology, 118, 104403.

Grandjean, G. (1994). Etude des structures crustales dans une portion de chaîne et de leur relation avec les bassins sédimentaires. Application aux Pyrénées occidentales. *Bulletin Des Centres de Recherches Exploration-Production Elf-Aquitaine*, *18*(2), 391–420.

Gregory, S., Barnett, M., Field, L., & Milodowski, A. (2019). Subsurface Microbial Hydrogen Cycling: Natural Occurrence and Implications for Industry. *Microorganisms*, *7*(2), 53. https://doi.org/10.3390/microorganisms7020053

Hainzl, S. (2004). Seismicity patterns of earthquake swarms due to fluid intrusion and stress triggering. *Geophysical Journal International*, *159*(3), 1090–1096. https://doi.org/10.1111/j.1365-246X.2004.02463.x

Halas, P., Dupuy, A., Franceschi, M., Bordmann, V., Fleury, J.-M., & Duclerc, D. (2021). Hydrogen gas in circular depressions in South Gironde, France: Flux, stock, or artefact? *Applied Geochemistry*, *127*, 104928. https://doi.org/10.1016/j.apgeochem.2021.104928

Hardebeck, J. L. (2012). Fluid-Driven Seismicity Response of the Rinconada Fault near Paso Robles, California, to the 2003 M 6.5 San Simeon Earthquake. *Bulletin of the Seismological Society of America*, *102*(1), 377–390. https://doi.org/10.1785/0120110169

Hinkle, M. E., Ryder, J. L., Sutley, S. J., & Botinelly, T. (1990). Production of sulfur gases and carbon dioxide by synthetic weathering of crushed drill cores from the Santa Cruz porphyry copper deposit near Casa Grande, Pinal County, Arizona. Journal of Geochemical Exploration, 38(1–2), 43–67. https://doi.org/10.1016/0375-6742(90)90092-O

Hirose, T., Kawagucci, S., & Suzuki, K. (2011). Mechanoradical H_2 generation during simulated faulting: Implications for an earthquake-driven subsurface biosphere: H_2 GENERATION DURING EARTHQUAKES. *Geophysical Research Letters*, *38*(17), n/a-n/a. https://doi.org/10.1029/2011GL048850

Jammes, S., Manatschal, G., Lavier, L., & Masini, E. (2009). Tectonosedimentary evolution related to extreme crustal thinning ahead of a propagating ocean: Example of the western Pyrenees: EXTREME CRUSTAL THINNING IN THE PYRENEES. *Tectonics*, *28*(4), n/a-n/a. https://doi.org/10.1029/2008TC002406

Jammes, S., Lavier, L., & Manatschal, G. (2010). Extreme crustal thinning in the Bay of Biscay and the Western Pyrenees: From observations to modeling: MODELIZATION OF EXTREME CRUSTAL THINNING. *Geochemistry, Geophysics, Geosystems*, *11*(10), n/a-n/a. https://doi.org/10.1029/2010GC003218

Johnson, J. E., Mienert, J., Plaza-Faverola, A., Vadakkepuliyambatta, S., Knies, J., Bünz, S., et al. (2015). Abiotic methane from ultraslow-spreading ridges can charge Arctic gas hydrates. *Geology*, *43*(5), 371–374. https://doi.org/10.1130/G36440.1

Kessler, A. J., Chen, Y.-J., Waite, D. W., Hutchinson, T., Koh, S., Popa, M. E., et al. (2019). Bacterial fermentation and respiration processes are uncoupled in anoxic permeable sediments. *Nature Microbiology*, *4*(6), 1014–1023. https://doi.org/10.1038/s41564-019-0391-z

Kita, I., Matsuo, S., & Wakita, H. (1982). H_2 generation by reaction between H_2O and crushed rock: An experimental study on H_2 degassing from the active fault zone. *Journal of Geophysical Research: Solid Earth*, *87*(B13), 10789–10795. https://doi.org/10.1029/JB087iB13p10789

Korotcenkov, G., Han, S. D., & Stetter, J. R. (2009). Review of Electrochemical Hydrogen Sensors. Chemical Reviews, 109(3), 1402–1433. https://doi.org/10.1021/cr800339k

Lacan, P. (2008). Activité sismotectonique plio-quaternaire de l'ouest des Pyrénées. https://tel.archives-ouvertes.fr/tel-01783939

Labaume, P., & Teixell, A., 2020, Evolution of salt structures of the Pyrenean rift (Chaînons Béarnais, France): From hyper-extension to tectonic inversion. Tectonophysics, 228451.

Lagabrielle, Y., & Bodinier, J.-L. (2008). Submarine reworking of exhumed subcontinental mantle rocks: field evidence from the Lherz peridotites, French Pyrenees: Cretaceous exhumation of pyrenean mantle. *Terra Nova*, *20*(1), 11–21. https://doi.org/10.1111/j.1365-3121.2007.00781.x

Lagabrielle, Y., Labaume, P., & de Saint Blanquat, M. (2010). Mantle exhumation, crustal denudation, and gravity tectonics during Cretaceous rifting in the Pyrenean realm (SW Europe): Insights from the geological setting of the lherzolite bodies: PYRENEAN LHERZOLITES, GRAVITY TECTONICS. *Tectonics*, *29*(4). https://doi.org/10.1029/2009TC002588

Lagabrielle, Y., Clerc, C., Vauchez, A., Lahfid, A., Labaume, P., Azambre, B., Fourcade, S., & Dautria, J. M., 2016, Very high geothermal gradient during mantle exhumation recorded in mylonitic marbles and carbonate breccias from a Mesozoic Pyrenean palaeomargin (Lherz area, North Pyrenean Zone, France). Comptes Rendus Géoscience, 348(3-4), 290-300.

Larin, N., Zgonnik, V., Rodina, S., Deville, E., Prinzhofer, A., & Larin, V. N. (2015a). Natural Molecular Hydrogen Seepage Associated with Surficial, Rounded Depressions on the European Craton in Russia. *Natural Resources Research*, *24*(3), 369–383. https://doi.org/10.1007/s11053-014-9257-5

Le Fur Balouet, S., (1985). Les séquences paléovolcaniques du domaine pyrénéen depuis le Stéphano-permien jusqu'au Crétacé: essai d'identification basé sur l'étude géochimique des éléments en traces (Doctoral dissertation), Thesis 3 ème Cycle, Paris VI, pp. 320.

Lescoutre, R., Tugend, J., Brune, S., Masini, E., & Manatschal, G., 2019, Thermal evolution of asymmetric hyperextended magma-poor rift systems: results from numerical modelling and Pyrenean field observations. Geochemistry, Geophysics, Geosystems. doi:10.1029/2019gc008600

Lescoutre, R., & Manatschal, G. (2020). Role of rift-inheritance and segmentation for orogenic evolution: example from the Pyrenean-Cantabrian systemRôle de l'héritage associé au rift et à sa segmentation pour l'évolution orogénique: exemple du système pyrénéo-cantabrique. Bulletin de la Société Géologique de France, 191(1).

Lewan, M. D. (1997). Experiments on the role of water in petroleum formation. *Geochimica et Cosmochimica Acta*, *61*(17), 3691–3723. https://doi.org/10.1016/S0016-7037(97)00176-2

Li, X., Krooss, B. M., Weniger, P., & Littke, R. (2017). Molecular hydrogen (H2) and light hydrocarbon gases generation from marine and lacustrine source rocks during closed-system laboratory pyrolysis experiments. *Journal of Analytical and Applied Pyrolysis*, *126*, 275–287. https://doi.org/10.1016/j.jaap.2017.05.019

Li, Y., Du, J., Wang, X., Zhou, X., Xie, C., & Cui, Y. (2013). Spatial Variations of Soil Gas Geochemistry in the Tangshan Area of Northern China. *Terrestrial, Atmospheric and Oceanic Sciences*, *24*(3), 323. https://doi.org/10.3319/TAO.2012.11.26.01(TT)

Lin, L.-H., Slater, G. F., Sherwood Lollar, B., Lacrampe-Couloume, G., & Onstott, T. C. (2005a). The yield and isotopic composition of radiolytic H2, a potential energy source for the deep subsurface biosphere. *Geochimica et Cosmochimica Acta*, *69*(4), 893–903. https://doi.org/10.1016/j.gca.2004.07.032

Lin, L.-H., Hall, J., Lippmann-Pipke, J., Ward, J. A., Sherwood Lollar, B., DeFlaun, M., et al. (2005b). Radiolytic H 2 in continental crust: Nuclear power for deep subsurface microbial communities: radiolytic H_2 in continental crust. Geochemistry, Geophysics, Geosystems, 6(7), n/a-n/a. https://doi.org/10.1029/2004GC000907

Lombardi, S., & Voltattorni, N. (2010). Rn, He and CO2 soil gas geochemistry for the study of active and inactive faults. *Applied Geochemistry*, *25*(8), 1206–1220. https://doi.org/10.1016/j.apgeochem.2010.05.006

Lorant, F., & Behar, F. (2002). Late Generation of Methane from Mature Kerogens. *Energy & Fuels*, *16*(2), 412–427. https://doi.org/10.1021/ef010126x

Malvoisin, B., Carlut, J., & Brunet, F. (2012). Serpentinization of oceanic peridotites: 1. A high-sensitivity method to monitor magnetite production in hydrothermal experiments. *Journal of Geophysical Research: Solid Earth*, *117*(B1). https://doi.org/10.1029/2011JB008612

Marcaillou, C., Muñoz, M., Vidal, O., Parra, T., & Harfouche, M. (2011). Mineralogical evidence for H2 degassing during serpentinization at 300°C/300bar. *Earth and Planetary Science Letters*, *303*(3–4), 281–290. https://doi.org/10.1016/j.epsl.2011.01.006

Masini, E., Manatschal, G., Tugend, J., Mohn, G., & Flament, J.-M. (2014). The tectono-sedimentary evolution of a hyper-extended rift basin: the example of the Arzacq–Mauléon rift system (Western Pyrenees, SW France). *International Journal of Earth Sciences*, *103*(6), 1569–1596. https://doi.org/10.1007/s00531-014-1023-8

Mayhew, L. E., Ellison, E. T., McCollom, T. M., Trainor, T. P., & Templeton, A. S. (2013). Hydrogen generation from low-temperature water–rock reactions. *Nature Geoscience*, *6*(6), 478–484. https://doi.org/10.1038/ngeo1825

McCarthy, J. H., & Reimer, G. M. (1986). Advances in soil gas geochemical exploration for natural resources: Some current examples and practices. *Journal of Geophysical Research: Solid Earth*, *91*(B12), 12327–12338. https://doi.org/10.1029/JB091iB12p12327

McCollom, T. M. (2013). Laboratory Simulations of Abiotic Hydrocarbon Formation in Earth's Deep Subsurface. Reviews in Mineralogy and Geochemistry, 75(1), 467–494. https://doi.org/10.2138/rmg.2013.75.15

McCollom, T. M., Klein, F., Robbins, M., Moskowitz, B., Berquó, T. S., Jöns, N., et al. (2016). Temperature trends for reaction rates, hydrogen generation, and partitioning of iron during experimental serpentinization of olivine. *Geochimica et Cosmochimica Acta*, *181*, 175–200. https://doi.org/10.1016/j.gca.2016.03.002

Meredith, L. K., Commane, R., Keenan, T. F., Klosterman, S. T., Munger, J. W., Templer, P. H., ... & Prinn, R. G. (2017). Ecosystem fluxes of hydrogen in a mid-latitude forest driven by soil microorganisms and plants. Global change biology, 23(2), 906-919.

Monnin, C., Chavagnac, V., Boulart, C., Ménez, B., Gérard, M., Gérard, E., et al. (2014). Fluid chemistry of the low temperature hyperalkaline hydrothermal system of Prony Bay (New Caledonia). Biogeosciences, 11(20), 5687–5706. https://doi.org/10.5194/bg-11-5687-2014

Moretti, I., Prinzhofer, A., Françolin, J., Pacheco, C., Rosanne, M., Rupin, F., & Mertens, J. (2021). Long-term monitoring of natural hydrogen superficial emissions in a brazilian cratonic environment. Sporadic large pulses versus daily periodic emissions. *International Journal of Hydrogen Energy*, *46*(5), 3615–3628. https://doi.org/10.1016/j.ijhydene.2020.11.026

Mouthereau, F., Filleaudeau, P.-Y., Vacherat, A., Pik, R., Lacombe, O., Fellin, M. G., et al. (2014). Placing limits to shortening evolution in the Pyrenees: Role of margin architecture and implications for the Iberia/Europe convergence: Plate convergence in the Pyrenees. *Tectonics*, *33*(12), 2283–2314. https://doi.org/10.1002/2014TC003663

Muñoz, J. A., 1992, Evolution of a continental collision belt; ECORS-Pyrenees crustal balanced cross-section. In K. R. Mcclay (Ed.), Thrust tectonics, (pp. 235–246). London, United Kingdom: Chapman & Hall

Muñoz, J.A., 2002, The Pyrenees. In: Gibbons, W., Moreno, T. (eds.). The Geology of Spain. The Geological Society of London, 370-385

Murray, J., Clément, A., Fritz, B., Schmittbuhl, J., Bordmann, V., & Fleury, J. M. (2020). Abiotic hydrogen generation from biotite-rich granite: A case study of the Soultz-sous-Forêts geothermal site, France. *Applied Geochemistry*, *119*, 104631. https://doi.org/10.1016/j.apgeochem.2020.104631

Neal, C., & Stanger, G. (1983). Hydrogen generation from mantle source rocks in Oman. Earth and Planetary Science Letters, 66, 315–320. https://doi.org/10.1016/0012-821X(83)90144-9

Noble, R. R. P., Lintern, M. J., Townley, B., Anand, R. R., Gray, D. G., & Reid, N. (2013). Metal migration at the North Miitel Ni sulphide deposit in the southern Yilgarn Craton: Part 3, gas and overview. Geochemistry: Exploration, Environment, Analysis, 13(2), 99–113. https://doi.org/10.1144/geochem2012-131

Novelli, P. C., Lang, P. M., Masarie, K. A., Hurst, D. F., Myers, R., & Elkins, J. W. (1999). Molecular hydrogen in the troposphere: Global distribution and budget. Journal of Geophysical Research: Atmospheres, 104(D23), 30427–30444. https://doi.org/10.1029/1999JD900788

Ortiz, A., Guillocheau, F., Lasseur, E., Briais, J., Robin, C., Serrano, O., & Fillon, C., 2020, Sediment routing system and sink preservation during the post-orogenic evolution of a retro-foreland basin: The case example of the North Pyrenean (Aquitaine, Bay of Biscay) Basins. Marine and Petroleum Geology, 112, 104085.

Oufi, O. (2002). Magnetic properties of variably serpentinized abyssal peridotites. *Journal of Geophysical Research*, *107*(B5), 2095. https://doi.org/10.1029/2001JB000549

Pedreira, D., Pulgar, J., Gallart, J., & Torné, M. (2007). Three-dimensional gravity and magnetic modeling of crustal indentation and wedging in the western Pyrenees-Cantabrian Mountains. *Journal of Geophysical Research: Solid Earth*, *112*(B12). https://doi.org/10.1029/2007JB005021

Pedrera, A., García-Senz, J., Ayala, C., Ruiz-Constán, A., Rodríguez-Fernández, L. R., Robador, A., & González Menéndez, L. (2017). Reconstruction of the Exhumed Mantle Across the North Iberian Margin by Crustal-Scale 3-D Gravity Inversion and Geological Cross Section: Mantle Along the Basque-Cantabrian Basin. Tectonics, 36(12), 3155–3177. https://doi.org/10.1002/2017TC004716

Pereira, A. J. S. C., Godinho, M. M., & Neves, L. J. P. F. (2010). On the influence of faulting on small-scale soil-gas radon variability: a case study in the Iberian Uranium Province. *Journal of Environmental Radioactivity*, *101*(10), 875–882. https://doi.org/10.1016/j.jenvrad.2010.05.014

Peters, J. W., Schut, G. J., Boyd, E. S., Mulder, D. W., Shepard, E. M., Broderick, J. B., et al. (2015). [FeFe]- and [NiFe]-hydrogenase diversity, mechanism, and maturation. *Biochimica et Biophysica Acta (BBA) - Molecular Cell Research*, *1853*(6), 1350–1369. https://doi.org/10.1016/j.bbamcr.2014.11.021

Polito, P. A., Clarke, J. D. A., Bone, Y., & Viellenave, J. (2002). A CO 2 –O 2 –light hydrocarbon–soil-gas anomaly above the Junction orogenic gold deposit: a potential, alternative exploration technique. Geochemistry: Exploration, Environment, Analysis, 2(4), 333–344. https://doi.org/10.1144/1467-787302-035

Potter, J., & Konnerup-Madsen, J. (2003). A review of the occurrence and origin of abiogenic hydrocarbons in igneous rocks. *Geological Society, London, Special Publications*, *214*(1), 151–173. https://doi.org/10.1144/GSL.SP.2003.214.01.10

Prinzhofer, A., Tahara Cissé, C. S., & Diallo, A. B. (2018). Discovery of a large accumulation of natural hydrogen in Bourakebougou (Mali). *International Journal of Hydrogen Energy*, *43*(42), 19315–19326. https://doi.org/10.1016/j.ijhydene.2018.08.193

Prinzhofer, A., Moretti, I., Françolin, J., Pacheco, C., D'Agostino, A., Werly, J., & Rupin, F. (2019). Natural hydrogen continuous emission from sedimentary basins: The example of a Brazilian H2-emitting structure. *International Journal of Hydrogen Energy*, *44*(12), 5676–5685. https://doi.org/10.1016/j.ijhydene.2019.01.119

Qureshi, A. A., Samad Beg, M. A., Ahmed, F., & Khan, H. A. (1988). Uranium exploration in Pakistan using alpha sensitive plastic films (ASPF). *International Journal of Radiation Applications and Instrumentation. Part D. Nuclear Tracks and Radiation Measurements*, *15*(1–4), 735–739. https://doi.org/10.1016/1359-0189(88)90240-3

Ravier, J., 1959, Le metamorphisme des terrains secondaires des Pyrenees, Memoires Soc. Geol. Fr. Nouv. Ser., (Vol. 38). Paris: Société géologique de France.

Reimann, C., Filzmoser, P., & Garrett, R. G. (2005). Background and threshold: critical comparison of methods of determination. *Science of The Total Environment*, *346*(1–3), 1–16. https://doi.org/10.1016/j.scitotenv.2004.11.023

Rigo, A., Béthoux, N., Masson, F., & Ritz, J.-F. (2008). Seismicity rate and wave-velocity variations as consequences of rainfall: the case of the catastrophic storm of September 2002 in the Nîmes Fault region (Gard, France). *Geophysical Journal International*, *173*(2), 473–482. https://doi.org/10.1111/j.1365-246X.2008.03718.x

Romanak, K. D., Bennett, P. C., Yang, C., & Hovorka, S. D. (2012). Process-based approach to CO 2 leakage detection by vadose zone gas monitoring at geologic CO 2 storage sites: process-based leakage detection. Geophysical Research Letters, 39(15). https://doi.org/10.1029/2012GL052426

Rossy, M., Azambre, B., & Albarède, F., 1992, REE and Sr/1bNd isotope geochemistry of the alkaline magmatism from the Cretaceous North Pyrenean Rift Zone (France-Spain). Chemical Geology, 97, 33–46. https://doi.org/10.1016/0009-2541(92)90134-Q

Roure, F., Choukroune, P., Berastegui, X., Munoz, J. A., Villien, A., Matheron, P., ... & Deramond, J. (1989). ECORS deep seismic data and balanced cross sections: Geometric constraints on the evolution of the Pyrenees. Tectonics, 8(1), 41-50.

Sahu, P., Mishra, D. P., Panigrahi, D. C., Jha, V., & Patnaik, R. L. (2013). Radon emanation from low-grade uranium ore. *Journal of Environmental Radioactivity*, *126*, 104–114. https://doi.org/10.1016/j.jenvrad.2013.07.014

Sainz-Garcia, A., Abarca, E., Rubi, V., & Grandia, F. (2017). Assessment of feasible strategies for seasonal underground hydrogen storage in a saline aquifer. *International Journal of Hydrogen Energy*, *42*(26), 16657–16666. https://doi.org/10.1016/j.ijhydene.2017.05.076

Saspiturry, N., Lahfid, A., Baudin, T., Guillou-Frottier, L., Razin, P., Issautier, B., et al. (2020). Paleogeothermal Gradients Across an Inverted Hyperextended Rift System: Example of the Mauléon Fossil Rift (Western Pyrenees). *Tectonics*, *39*(10). https://doi.org/10.1029/2020TC006206

Sato, M., Sutton, A. J., & McGee, K. A. (1985). Anomalous hydrogen emissions from the San Andreas fault observed at the Cienega Winery, central California. *Pure and Applied Geophysics PAGEOPH*, *122*(2–4), 376–391. https://doi.org/10.1007/BF00874606

Sauvage, J. F., Flinders, A., Spivack, A. J., Pockalny, R., Dunlea, A. G., Anderson, C. H., et al. (2021). The contribution of water radiolysis to marine sedimentary life. Nature Communications, 12(1), 1297. https://doi.org/10.1038/s41467-021-21218-z

Schrenk, M. O., Brazelton, W. J., & Lang, S. Q. (2013). Serpentinization, Carbon, and Deep Life. Reviews in Mineralogy and Geochemistry, 75(1), 575–606. https://doi.org/10.2138/rmg.2013.75.18

Schwartz, E., & Friedrich, B. (2006). The H2-metabolizing prokaryotes. *The Prokaryotes*, *7*, 496–563. https://doi.org/10.1007/0-387-30742-7_17

Sherwood Lollar, B. S., Heuer, V. B., McDermott, J., Tille, S., Warr, O., Moran, J. J., ... & Hinrichs, K. U. (2021). A window into the abiotic carbon cycle–Acetate and formate in fracture waters in 2.7 billion year-old host rocks of the Canadian Shield. Geochimica et Cosmochimica Acta, 294, 295-314.

Sherwood Lollar, B. S., Lacrampe-Couloume, G., Slater, G. F., Ward, J., Moser, D. P., & Gihring, T. M. (2006). Unravelling abiogenic and biogenic sources of methane in the Earth's deep subsurface. *Chemical Geology*, 12. https://doi.org/10.1016/j.chemgeo.2005.09.027

Sherwood Lollar, B. S., Onstott, T. C., Lacrampe-Couloume, G., & Ballentine, C. J. (2014). The contribution of the Precambrian continental lithosphere to global H2 production. Nature, 516(7531), 379–382. https://doi.org/10.1038/nature14017

Sibson, R. (1981). A brief description of natural neighbour interpolation. *Interpreting Multivariate Data*.

Sinclair, A. J. (1991). A fundamental approach to threshold estimation in exploration geochemistry: probability plots revisited. *Journal of Geochemical Exploration*, *41*(1–2), 1–22. https://doi.org/10.1016/0375-6742(91)90071-2

Sipma, J., Henstra, A. M., Parshina, S. N., Lens, P. N. L., Lettinga, G., & Stams, A. J. M. (2006). Microbial CO Conversions with Applications in Synthesis Gas Purification and Bio-Desulfurization. *Critical Reviews in Biotechnology*, *26*(1), 41–65. https://doi.org/10.1080/07388550500513974

Smith, N. J. P., Shepherd, T. J., Styles, M. T., & Williams, G. M. (2005). Hydrogen exploration: a review of global hydrogen accumulations and implications for prospective areas in NW Europe. *Geological Society, London, Petroleum Geology Conference Series*, *6*(1), 349–358. https://doi.org/10.1144/0060349

Souriau, A., Rigo, A., Sylvander, M., Benahmed, S., & Grimaud, F. (2014). Seismicity in central-western Pyrenees (France): A consequence of the subsidence of dense exhumed bodies. Tectonophysics, 621, 123–131. https://doi.org/10.1016/j.tecto.2014.02.008

Sugisaki, R., Ido, M., Takeda, H., Isobe, Y., Hayashi, Y., Nakamura, N., et al. (1983). Origin of Hydrogen and Carbon Dioxide in Fault Gases and Its Relation to Fault Activity. *The Journal of Geology*, *91*(3), 239–258. https://doi.org/10.1086/628769

Tarkowski, R. (2019). Underground hydrogen storage: Characteristics and prospects. *Renewable and Sustainable Energy Reviews*, *105*, 86–94. https://doi.org/10.1016/j.rser.2019.01.051

Teixell, A., 1998, Crustal structure and orogenic material budget in the west central Pyrenees. Tectonics, 17(3), 395-406.

Teixell, A., Labaume, P., & Lagabrielle, Y. (2016). The crustal evolution of the west-central Pyrenees revisited: Inferences from a new kinematic scenario. *Comptes Rendus Geoscience*, *348*(3–4), 257–267. https://doi.org/10.1016/j.crte.2015.10.010

Teixell, A., Labaume, P., Ayarza, P., Espurt, N., de Saint Blanquat, M., & Lagabrielle, Y., 2018, Crustal structure and evolution of the Pyrenean-Cantabrian belt: A review and new interpretations from recent concepts and data. Tectonophysics, 724-725, 146–170. https://doi.org/10.1016/j.tecto.2018.01.009

Thauer, R. K., Klein, A. R., & Hartmann, G. C. (1996). Reactions with Molecular Hydrogen in Microorganisms: Evidence for a Purely Organic Hydrogenation Catalyst. *Chemical Reviews*, *96*(7), 3031–3042. https://doi.org/10.1021/cr9500601

Toft, P. B., Arkani-Hamed, J., & Haggerty, S. E. (1990). The effects of serpentinization on density and magnetic susceptibility: a petrophysical model. *Physics of the Earth and Planetary Interiors*, *65*(1–2), 137–157. https://doi.org/10.1016/0031-9201(90)90082-9

Toutain, J.-P., & Baubron, J.-C. (1999). Gas geochemistry and seismotectonics: a review. *Tectonophysics*, *304*(1–2), 1–27. https://doi.org/10.1016/S0040-1951(98)00295-9

Truche, L., & Bazarkina, E. F. (2019). Natural hydrogen the fuel of the 21 st century. *E3S Web of Conferences*, *98*, 03006. https://doi.org/10.1051/e3sconf/20199803006

Truche, L., Joubert, G., Dargent, M., Martz, P., Cathelineau, M., Rigaudier, T., & Quirt, D. (2018). Clay minerals trap hydrogen in the Earth's crust: Evidence from the Cigar Lake uranium deposit, Athabasca. *Earth and Planetary Science Letters*, *493*, 186–197. https://doi.org/10.1016/j.epsl.2018.04.038

Truche, L., McCollom, T. M., & Martinez, I. (2020). Hydrogen and abiotic hydrocarbons: molecules that change the world. Elements: An International Magazine of Mineralogy, Geochemistry, and Petrology, 16(1), 13-18.

Tugend, J., Manatschal, G., Kusznir, N. J., Masini, E., Mohn, G., & Thinon, I. (2014). Formation and deformation of hyperextended rift systems: Insights from rift domain mapping in the Bay of Biscay-Pyrenees. *Tectonics*, *33*(7), 1239–1276. https://doi.org/10.1002/2014TC003529

Tugend, J., Manatschal, G., & Kusznir, N. J., 2015b, Spatial and temporal evolution of hyperextended rift systems: Implication for the nature, kinematics, and timing of the Iberian-European plate boundary. Geology, 43(1), 15-18. https://doi.org/10.1130/G36072.1

Vacher, P., & Souriau, A. (2001). A three-dimensional model of the Pyrenean deep structure based on gravity modelling, seismic images and petrological constraints. *Geophysical Journal International*, *145*(2), 460–470. https://doi.org/10.1046/j.0956-540x.2001.01393.x

Vacquand, C., Deville, E., Beaumont, V., Guyot, F., Sissmann, O., Pillot, D., et al. (2018). Reduced gas seepages in ophiolitic complexes: Evidences for multiple origins of the H2-CH4-N2 gas mixtures. Geochimica et Cosmochimica Acta, 223, 437–461. https://doi.org/10.1016/j.gca.2017.12.018

Vandenborre, J., Truche, L., Costagliola, A., Craff, E., Blain, G., Baty, V., Haddad, F. and Fattahi, M., 2021. Carboxylate anion generation in aqueous solution from carbonate radiolysis, a potential route for abiotic organic acid synthesis on Earth and beyond. Earth and Planetary Science Letters, 564, p.116892.

Vergés, J., Millán, H., Roca, E., Muñoz, J. A., Marzo, M., Cirés, J., et al., 1995, Eastern Pyrenees and related foreland basins: pre-, syn- and post-collisional crustal-scale cross-sections. Marine and Petroleum Geology, 12, 903–915. https://doi.org/10.1016/0264-8172(95)98854-X

Vergés, J., & García-Senz, J., 2001, Mesozoic evolution and Cainozoic inversion of the Pyrenean rift. In P. A. Ziegler, et al. (Eds.), Peri-Tethyan Rift/Wrench Basins and Passive Margins, mémoire, (pp. 187–212).

Vergés, J., Fernàndez, M., & Martìnez, A. (2002). The Pyrenean orogen: pre-, syn-, and post-collisional evolution. *Journal of the Virtual Explorer*, *08*. https://doi.org/10.3809/jvirtex.2002.00058

Wang, Y., Chevrot, S., Monteiller, V., Komatitsch, D., Mouthereau, F., Manatschal, G., et al. (2016). The deep roots of the western Pyrenees revealed by full waveform inversion of teleseismic P waves. *Geology*, *44*(6), 475–478. https://doi.org/10.1130/G37812.1

Warren, J., 2016. Gases in evaporites: part 2 of 3: nature, distribution and sources. Salty Matters reports.

Worman, S. L., Pratson, L. F., Karson, J. A., & Klein, E. M. (2016). Global rate and distribution of H 2 gas produced by serpentinization within oceanic lithosphere: H_2 formation in ocean lithosphere. Geophysical Research Letters, 43(12), 6435–6443. https://doi.org/10.1002/2016GL069066

Worman, S. L., Pratson, L. F., Karson, J. A., & Schlesinger, W. H. (2020). Abiotic hydrogen (H_2) sources and sinks near the Mid-Ocean Ridge (MOR) with implications for the subseafloor biosphere. Proceedings of the National Academy of Sciences, 117(24), 13283–13293. https://doi.org/10.1073/pnas.2002619117

Xiang, Y., Sun, X., Liu, D., Yan, L., Wang, B., & Gao, X. (2020). Spatial Distribution of Rn, CO2, Hg, and H2 Concentrations in Soil Gas Across a Thrust Fault in Xinjiang, China. Frontiers in Earth Science, 8, 554924. https://doi.org/10.3389/feart.2020.554924

Zgonnik, V., Beaumont, V., Deville, E., Larin, N., Pillot, D., & Farrell, K. M. (2015). Evidence for natural molecular hydrogen seepage associated with Carolina bays (surficial, ovoid depressions on the Atlantic Coastal Plain, Province of the USA). *Progress in Earth and Planetary Science*, *2*(1), 31. https://doi.org/10.1186/s40645-015-0062-5

Zivar, D., Kumar, S., & Foroozesh, J. (2020). Underground hydrogen storage: A comprehensive review. *International Journal of Hydrogen Energy*, S0360319920331426. https://doi.org/10.1016/j.ijhydene.2020.08.138